

**TOWSON UNIVERSITY
OFFICE OF GRADUATE STUDIES**

**AN ANALYSIS OF THE INFLUENCE OF PRECEDING PRECIPITATION ON
THE SIGNATURE OF BALTIMORE'S SURFACE URBAN HEAT ISLAND**

**by
Ryan Charles Lingo**

**A thesis
Presented to the faculty of
Towson University
in partial fulfillment
of the requirements for the degree Master of Arts
Department of Geography and Environmental Planning

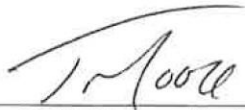
Towson University
Towson, Maryland 21252**

May, 2018

**TOWSON UNIVERSITY
OFFICE OF GRADUATE STUDIES**

THESIS APPROVAL PAGE

This is to certify that the thesis prepared by Ryan Charles Lingo, entitled AN ANALYSIS OF THE INFLUENCE OF PRECEDING PRECIPITATION ON THE SIGNATURE OF BALTIMORE'S SURFACE URBAN HEAT ISLAND, had been approved by the thesis committee as satisfactorily completing the thesis requirements for the degree Master of Arts.



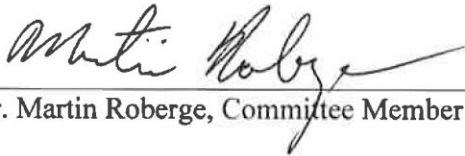
Dr. Todd Moore, Chair, Thesis Committee

5/4/2018
Date



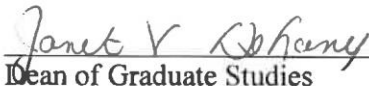
Dr. Paporn Thebpanya, Committee Member

5/4/2018
Date



Dr. Martin Roberge, Committee Member

5/3/2018
Date



Dean of Graduate Studies

5-8-18
Date

Acknowledgements

Dr. Todd Moore

Dr. Paporn Thebpanya

Dr. Martin Roberge

Dr. John M. Morgan, III

Dr. Nathaniel Burtch

Dr. Virginia Thompson

Julia Heslin

and all of my family and friends for their listening ears, encouragement, and love.

Abstract

AN ANALYSIS OF THE INFLUENCE OF PRECEDING PRECIPITATION ON THE SIGNATURE OF SURFACE URBAN HEAT ISLANDS

Ryan Charles Lingo

Surface Urban Heat Islands (SUHI) are urban areas where temperatures exceed that of their rural counterparts. SUHIs are caused by alterations of the land surface by humans, generally from natural vegetated surfaces to urban surfaces (Zhou et al., 2014). SUHIs have been studied using multiple methods (Voogt & Oke, 2003). One method involves collecting satellite images using specific criteria. This includes percent cloud cover (CC), time of day, season, wind speed, and synoptic setup. These studies overlook preceding precipitation and its impact on the overall SUHI analysis. This study collected eight satellite images of Baltimore County, Maryland from 1994 to 2016. Four satellite scenes had preceding precipitation occur within three days of satellite acquisition. Four satellite scenes had no preceding precipitation. Land surface temperature (LST), Normalized Difference Vegetation Index (NDVI), Normalized Difference Built-Up Index (NDBI), and Normalized Difference Water Index (NDWI) were calculated for each scene. LST was regressed on NDVI, NDBI, and NDWI. Both NDBI and NDWI were positively correlated with LST. NDVI had a negative correlation. On average the explanatory power of NDVI, NDBI, and NDWI decreased for scenes with preceding precipitation. The Getis-Ord G_i^* statistic showed no difference in spatial clustering of hot and cold LST for all images.

Table of Contents

List of Tables	vii
List of Figures	viii
Chapter One: Introduction	1
1.1 Introduction	1
1.2 Chapter 1 Tables.....	3
1.3 Chapter 1 Figures	3
Chapter Two: Literature Review	4
2.1 Definitions and Causes.....	4
2.2 History of UHI	4
2.3 Types of UHI and methods of documenting	6
2.4 SUHI Studies.....	7
2.4.1 Magnitudes of the SUHI.....	7
2.4.2 Temporal and spatial changes of the SUHI.....	8
2.4.3 LST and LULC Relationships	8
2.5 Problems with Today's Methods of Inquiry and a Need for Accurate Documentation of the SUHI.....	9
2.6 Chapter 2 Tables.....	12
Chapter Three: Data and Methods	13
3.1 Study Area.....	13
3.2 Data Sources.....	13
3.2.1 Study Area Shapefile	13
3.2.2 Precipitation Data	13
3.2.3 Satellite Imagery	14
3.3 Preprocessing Satellite Scenes	15
3.3.1 Landsat 5 Scenes	16
3.3.2 Landsat 8 Scenes	16
3.4 Land Surface Temperature Retrieval	17
3.2.1 NDVI	17
3.2.2 Emissivity	17
3.2.3 Thermal Function	17
3.5 SUHI Analysis.....	19

3.5.1 Does preceding precipitation influence the magnitude of Baltimore's SUHI?	19
3.5.2 Does preceding precipitation influence the clustering of micro SUHIs in Baltimore?	20
3.5.3 Does preceding precipitation influence the relationships between LST, NDVI, NDBI, NDWI in Baltimore?	21
3.6 Chapter 3 Tables	22
3.7 Chapter 3 Figures	23
Chapter Four: Results	28
4.1 Overview of Baltimore's SUHI	28
4.2 SUHI Magnitude	29
4.3 Clustering of LST	30
4.4 Landcover/LST Relationship	31
4.5 Chapter 4 Tables	33
4.6 Chapter 4 Figures	38
Chapter Five: Discussion	44
5.1 Discussion of Research Questions	44
5.2 Further Research	46
Chapter Six: Summary	49
Appendix A	51
Appendix B	63
Literature Cited	66
Curriculum Vitae	75

List of Tables

Table 1.1 Different characteristics used to select satellite imagery.....	3
Table 2.1 Examples of variables expressed in the surface energy balance.....	12
Table 2.2 Sample of satellites and their thermal bands used in quantifying the SUHI....	12
Table 3.1 Selected satellite scenes.....	22
Table 4.1 LST descriptive statistics. Mean, maximum, minimum, and standard deviation calculated for all scenes.....	33
Table 4.2. SUHI magnitude statistics.....	34
Table 4.3 Coefficient of determination, R, and slope coefficient values for all selected scenes.....	35
Table 4.4. NDVI descriptive statistics for all images.....	36
Table 4.5. NDBI descriptive statistics for all images.....	36
Table 4.6. NDWI descriptive statistics for all images.....	37

List of Figures

Figure 1.1 Météo France/Cécile de Munck urban heat island of Paris.....	3
Figure 3.1. Study area color composite and Baltimore County and City combined polygons for the study area.....	23
Figure 3.2 represents the process for calculating LST for a specific area.....	24
Figure 3.3 Idrisi Macro Language (IML) code used to calculate NDVI and emissivity.....	24
Figure 3.4 shows the prompts used to run the thermal conversion module.....	25
Figure 3.5 Reclassification of urban and non-urban pixels for 2 July 2016 using the CLUSTER module.....	26
Figure 3.6 shows the Regress module for calculating the linear regression for NDVI, NDBI, NDWI, and LST.....	27
Figure 3.7. LST transect location, 2 July 2016. The transect that extends from Gwynns Falls to Patterson Park and southeast toward the Chesapeake Bay.....	27
Figure 4.1. LST calculated for all Landsat scenes.....	38
Figure 4.2. LST transects. Each transect runs from Gwynn Falls to Druid Park to Patterson Park and south towards the Bay. See Figure 3.7.....	39
Figure 4.3 Getis-Ord Gi* spatial clustering statistic shows the confidence intervals (CI) of clustering of high and low LST.....	40
Figure 4.4. Normalized Difference Vegetation Index (NDVI) calculated for all Landsat scenes.....	41
Figure 4.5 Normalized Difference Built-up Index (NDBI) calculated for all Landsat scenes.....	42

Figure 4.6. Normalized Difference Water Index (NDWI) calculated for all Landsat

scenes.....43

Chapter One: Introduction

1.1 Introduction

Urban heat islands (UHI) are urban areas where temperatures exceed that of their rural counterparts (Figure 1.1). There are two atmospheric UHIs (Miao et al., 2009; Steeneveld et al., 2011), which include the urban canopy layer UHI and the urban boundary layer UHI (Voogt & Oke, 2003), and a surface urban heat island (SUHI) (Matson, 1978; Hafner, 1999; Imhoff et al., 2010; Peng et al., 2011; Pearsall, 2017).

UHIs are caused by alterations of the land surface by humans, generally from natural vegetated surfaces to urban surfaces (Rizwan et al., 2007; Zhou et al., 2014). These changes alter the surface energy balance (Rizwan et al., 2007), ultimately changing the land surface temperature (LST). It is important to study UHIs because, with increasing anthropogenic warming (IPCC, 2013), urban areas will likely experience disproportionately high rates of heat stress (CDC, 2006; Anderson & Bell, 2011; Fischer et al., 2012; Romero-Lankao, et al., 2012).

SUHI studies have quantified their magnitude (i.e., the difference in LST between the urban area and surrounding rural areas) (e.g., Matson et al., 1978; Balling & Brazel, 1987; Han-qui & Ben-qing, 2004; Imhoff et al., 2010; Liu & Zhang, 2011; Peng et al., 2011; Arnfield, 2013; Zhang et al, 2013; Effat & Hassan, 2014; Mills, 2014; Alghamdi & Moore, 2015), documented their spatial and temporal changes (e.g., Hu & Brunsell, 2013; Effat & Hassan, 2014; Wang et al., 2015), and evaluated associations between LST and a suite of land use/land cover (LULC) indices, such as the Normalized Difference Vegetation Index (NDVI), the Normalized Difference Built-up Index (NDBI), and the Normalized Difference Water Index (NDWI) (e.g., Becker & Li, 1995; Amiri et al., 2009; Deng & Wu, 2013; Zhou et al., 2013; Heusinkveld et al., 2014; Zhou et al.,

2014; Ali et al., 2017). To ensure accurate and consistent measurement of the SUHIs, these studies and others select satellite images that meet certain criteria. Many studies, for example, select images with similar percent cloud cover (CC), time of day, season, wind speed, and synoptic setup over the proposed area of study (Table 1.1).

However, the criteria that these studies use for scene selection fail to account for the potential influence of preceding precipitation on the magnitude of SUHIs, the temporal and spatial characteristics of SUHIs, and the relationships between LST and LULC indices. Studies have shown that water on pavement may possibly reduce the magnitude of heating that would occur on dry land surfaces (Yamagata et al., 2008; Nakayama & Fujita, 2010) and that wet surfaces may cause unsuitable and unreliable classification of satellite images (Rajasekar & Weng, 2009). The potential influence of preceding precipitation on SUHIs, and the lack of studies that consider preceding precipitation in their image selection process, present a need to evaluate the influence of preceding precipitation on the SUHI.

The purpose of this study is to evaluate the influence of preceding precipitation on the SUHI signature in Baltimore, Maryland. The research questions guiding this study are:

- 1) Does preceding precipitation influence the magnitude of Baltimore's SUHI?
- 2) Does preceding precipitation influence the clustering of micro SUHIs with Baltimore?
- 3) Does preceding precipitation influence the relationships between LST, NDVI, NDBI, NDWI in Baltimore?

1.2 Chapter 1 Tables

Table 1.1 shows different characteristics used to select satellite imagery. These include % cloud cover (CC), time of [day], season, wind, and weather type (synoptic).

Author	% Cloud Cover	Time of Day	Day and Night	Season	Wind	Synoptic
Rivera et al., 2018	x			x	x	
Pearsall, 2017		x				
Nassar et al., 2016	x	x	x	x	x	
Hu & Brunsell, 2015	x		x			
Effat & Hassan, 2014		x		x		
Zhou et al., 2014	x	x	x			
Lazzarini et al., 2013	x	x	x	x	x	
Li et al., 2013			x	x	x	
Schwarz et al., 2013		x	x			
Zhou et al., 2013	x	x	x			
Huang et al., 2011		x	x			
Imhoff et al., 2011	x	x	x			
Peng et al., 2011	x	x	x			
Tomlinson et al., 2011	x	x	x			x
Zhou et al., 2011	x	x	x			

1.3 Chapter 1 Figures

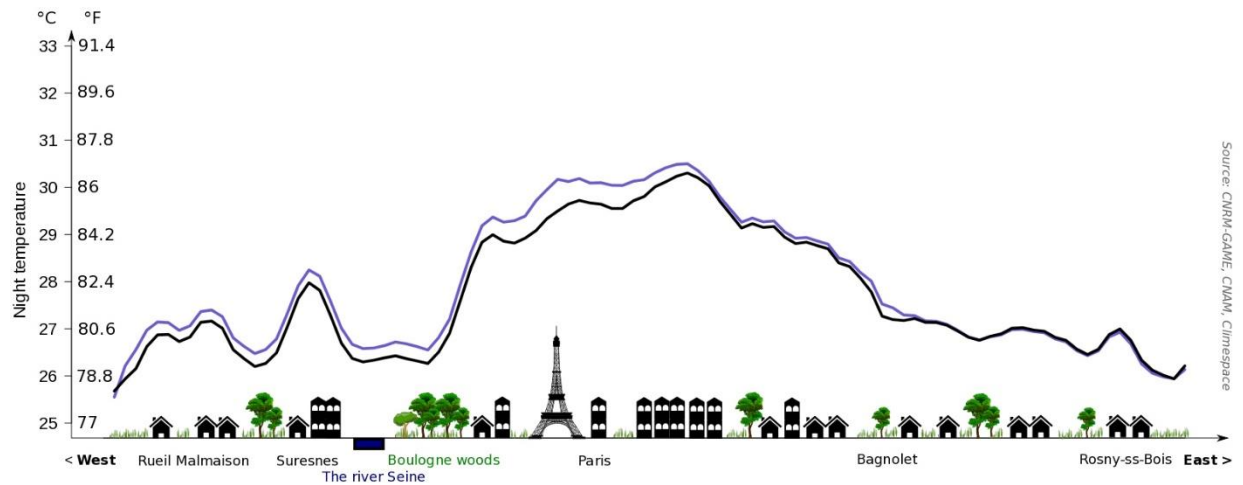


Figure 1.1 Météo France/Cécile de Munck urban heat island of Paris (Voiland, 2010).

Chapter Two: Literature Review

2.1 Definitions and Causes

SUHIs are formed when the urban thermal radiance (Voogt & Oke, 2003), otherwise known as radiometric temperature (T_{sr}) or skin temperature (Becker & Li, 1995), exceeds those of the surrounding rural areas. LULC changes lead to the development of SUHIs by altering components of the surface energy balance (Taha, 1997; Grimmond, 2007; Miao et al., 2007; Rizwan et al., 2007; Zhou et al., 2010; Husinkveld et al., 2014; Zhou et al., 2014), which can be represented by (Oke, 1988, Rizwan et al., 2007):

$$Q^* + Q_F = Q_H + Q_E + \Delta Q_S + \Delta Q_A \quad (1)$$

Where, Q^* is the net all wave radiation, Q_F is heat release by combustion, Q_H is the turbulent sensible heat flux density, Q_E is the turbulent latent heat flux, ΔQ_S is the net heat storage, and ΔQ_A is the net moisture advection. For examples of each variable, see Table 2.1 as described by Rizwan (2007). LULC changes may lead to increased sensible heating (Q_H) and decreased latent heating (Q_E), which increase the urban areas sensible temperature (Oke, 1988; Rizwan, 2007).

2.2 History of UHI

Urbanization and its impact on the climate have been extensively studied throughout the 20th and 21st centuries (Howard, 1883; Matson, 1978; Oke, 1988; Hafner, 1999; Arnfield, 2003; Stone, 2007; Bounoua et al., 2009; Imhoff et al., 2010; Peng et al., 2011; Mahmood et al. 2014; Bounoua, 2017; Pearsall, 2017). These studies, and others, noted the significant spatial and temporal differences in temperatures between rural and urban locations, known as the UHI. Manley (1958) was the first to call the temperature

difference between urban and rural areas the UHI. Urban climatology (Mills, 2014), though, has been studied since the late 1800's, particularly the UHI, most notably by Luke Howard (Howard, 1883). Howard wrote about the difference between urban and rural temperatures in London, United Kingdom. By the 1900's measurements were being collected on different observed meteorological variables (Bornstein, 1968; Mills, 2014) and then, after the mid-19th century, studies began to use statistics to quantify different processes like latent and sensible heat fluxes (Mills, 2014) and to create different numerical models (Myrup, 1969).

Methods for the spatial analysis of the SUHI have changed over time (Voogt & Oke, 2003; Tomlinson et al., 2011; Becker & Zhao-Liang, 2015). Beginning in the 1970's, with the advent of computers, satellites, and Geographic Information Systems (GIS), (Tomlinson et al., 2011; Mills, 2014) the UHI began to be seen from a spatial perspective. Matson (1978) was able to capture St. Louis, Baltimore, and Washington's SUHI. Meanwhile, with a more robust understanding of UHI (Mills, 2014), Urban climatology vocabulary were expanded upon (e.g. urban surface, land cover, street dimensions). Scholars then studied urban climatology, including the UHI, with statistics and numerical computer models, for instance Myrup (1969), which utilized mesoscale and microscale meteorological variables. Effects on different types of land cover classifications (Voogt & Oke, 2003; Mills, 2014) and spatial and temporal patterns of the UHI (Rao, 1972; Matson, 1978; Imhoff et al., 2010; Sobrino et al., 2013; Zhou et al., 2014) were further studied. These methods are still utilized today but being applied to look at mitigation techniques (Battaglia et al., 2014) and socioeconomic impacts

(Pearsall, 2017). See Arnfield (2003), Voogt and Oke (2003), Souch and Grimmond (2006), and Mills (2014) for additional thorough reviews of the history of UHI research.

2.3 Types of UHI and methods of documenting

Methods for studying UHI vary. For the atmospheric UHIs, stationary or fixed mast weather stations (Sobrino, 2013; Noro et al., 2015), weather balloon launches (Sobrino, 2013), and mobile (bicycle) transects (Hart & Sailor, 2009; Busato et al., 2014; Heusinkveld et al., 2014) have been used. While these methods provide continuous or near-continuous temporal coverage, they lack in spatial coverage. For instance, Busato et al. (2014) studied the UHI of Padua, Italy by running an 18-kilometer transect. Variation in temperature was noted along this transect, but the study was unable to document temperature variation for any other areas of the UHI. Collecting transects and discrete points leaves scientists interpolating temperature data instead of having an accurate spatial depiction of different areas. Representation of the atmospheric UHI is often limited in spatial extent because of this.

For SUHI, thermal remote sensing is used to capture an area in space and time using different wavelengths of the electromagnetic (EM) spectrum. Table 2.2 gives examples of satellites and their different thermal wavelengths. These images capture the spatial variability of the SUHI (Rao, 1972; Matson, 1978; Hafner, 1999; Imhoff et al. 2010; Peng et al. 2011; Pearsall, 2017), but they do not offer continuous temporal coverage like fixed weather stations. Multiple satellite images can be obtained to capture change over time (Mitraka et al., 2015). A study by Li et al. (2012) created a time series of images that illustrated temporal and spatial variability of LULC and the SUHI in

Shanghai, China. It was shown that LULC caused changes to the SUHI over space and time.

Thermal remote sensing methods for studying the SUHI have limitations (Mirzaei & Haghighat, 2010). Differing directions of thermal radiance will change depending on the dimensionality within the city. For instance, buildings casting shadows over an area will affect the amount of radiation that reflects back to the remote sensing instrument. The thermal radiance coming off the city is also going to be affected by surface radiance and thermodynamic properties. Parham Mirzaei and Haghighat (2010) state, “The main technical concern in this approach is nonetheless that the surface temperature measured by sensors only relates to the spatial patterns of upward thermal radiance received by the remote sensors (2010, p. 2,193).” Obtaining high resolution images for study also tends to be expensive.

2.4 SUHI Studies

Despite its limitations, remote sensing is a widely used method to study SUHIs. The relevant body of literature on SUHIs can be organized into the following themes: magnitude of SUHIs, change over time of SUHIs, LST and LULC relationships, and LST and socio-economic relationships.

2.4.1 Magnitudes of the SUHI

SUHI magnitude varies across space, within and between cities (Balling & Brazel, 1987; Gaffin et al., 2008). They change within different biomes and geographical locations (Chen et al., 2006; Imhoff et al., 2010; Zhou et al., 2014; Picón et al., 2017), city size (Oke, 1973), different types of materials within cities (Stewart & Oke, 2012; Zinzi & Carnielo, 2017), seasons (Chen et al., 2006; Cui & De Foy, 2012) and elevation

(Scott et al., 2017). For example, a temperate rainforest SUHI averages about 7°C to 9°C while a savannah averages about 4°C to 6°C (Imhoff, 2010).

2.4.2 Temporal and spatial changes of the SUHI

SUHIs change over time (Wilby, 2003; Alghamdi & Moore, 2015; Rivera et al., 2017), depending on population growth in the particular city (Oke, 1973; Zhang, 2013), change in built-up environment (Imhoff, 2010, Han-qiu & Ben-qing, 2004) change in vegetation (Weng et al, 2004; Zhang, 2013), and changes in albedo (Weng et al., 2004). These changes occur at the daily (Scott et al., 2017), seasonal (Zhou et al., 2014) and decadal time scales (Streutker, 2003).

Changes over time affect the spatial signature of the SUHI. As population increases, so too does the built-up environment (Grimmond, 2007). The spatial signature changes because of the different land cover types (Zhou & Cadenasso, 2011) and locations. For instance, Balling and Brazel (1987) noted a temperature difference in the SUHI in Phoenix, Arizona. The southwestern portion of the city had the highest recorded temperatures while to the north, where there was a greater elevation, temperatures were lower. Grimmond (2007) noted that the microclimates of an urban area can change quickly (e.g. a park on one side of the street and buildings on the other), ultimately changing the spatial signature.

2.4.3 LST and LULC Relationships

LULC change affects LST (Chen et al., 2006; Lu & Weng, 2006; Yuan & Bauer, 2007; Zhou et al., 2014). Depending on the type of land cover, LST will either increase or decrease. With a lack of vegetation, LST will no longer have a supply of latent heat and sensible heat will increase, whereas in a desert, there is a lack of vegetation, and LST will

tend to be lower in the urban areas than the surrounding rural areas (Lazzarini et al., 2013). There have been positive correlations found between vegetation (measured by NDVI) and LST (Carlson & Arthur, 2000; Zhou et al., 2014; Ali et al., 2017) which change due to the seasonal variation in temperature and vegetation in North America (Sun & Kafatos, 2007). Positive correlations are found in winter when vegetation cover is at its lowest and negative in summer when vegetation is at its greatest within UHIs. There have been positive correlations between NDBI, or built-up area, and LST (Bahi et al., 2016; Macarof & Statescu, 2017) and negative correlations between NDWI and LST (Ali et al., 2017). NDBI, NDWI, and LST correlations are affected by the amount of vegetation within cities, which means they will change during different seasons (Mathew et al., 2017). On average, LST tends to increase with urban characteristics like commercial and industrial buildings (Rinner & Hussain, 2011).

2.5 Problems with Today's Methods of Inquiry and a Need for Accurate Documentation of the SUHI

When studying the SUHI, researchers often-select satellite images that meet certain criteria (Table 1.1), but none to my knowledge have used preceding precipitation as a criterion. Preceding precipitation can cause decreases in temperatures on the surface of low albedo and impervious pavement (e.g. blacktop) (Hendel et al., 2014). With the addition of water, increases in latent heat flux and decreases in sensible heat flux can occur and cause surfaces to cool. Experimental studies have verified that water on pavement will reduce the magnitude of sensible heat (Yamagata et al., 2008; Nakayama & Fujita, 2010). This effect could possibly alter the magnitude of the SUHI, the spatial clustering of the SUHI, and the relationships between LST and land cover indices.

It is practical to explore the possible influence that preceding precipitation has on the signature of the SUHI, especially in cities that are commonly the focus of study. Baltimore's SUHI has been made apparent by numerous studies (e.g., Brazel et al., 2000; Zhou et al., 2011; Scott et al., 2017). In certain downtown areas, the LST can vary by as much as 5 °C to 10 °C over relatively short distances depending on the change in LULC (Scott et al., 2017). The lack of vegetation, which has been linked to areas of lower income (Harlan et al., 2007), causes LST to increase within Baltimore. In summer months, Baltimore sees a less variable minimum temperature and a mean temperature for the season around 21.7 °C. During winter the SUHI has its greatest magnitude.

Links between LST and LULC indices in Baltimore have been frequently studied (Imhoff et al., 2010; Li & Bou-Zeid, 2013, Hardin et al., 2017; Tang et al., 2017). Huang et al. (2011) found that 70% of the variance in LST temperature could be explained by buildings and vegetation. Zhou et al. (2014) found that impervious surfaces increase LST and vegetation decreases LST. Baltimore's SUHI has been studied, but no one has sought to analyze the impact of preceding precipitation on its magnitude and spatial clustering, or on the links between LST and LC indices.

Understanding the impact of preceding precipitation in Baltimore and in other urban areas will improve our ability to accurately and consistently document the magnitude of the SUHI, the spatial signature of the SUHI, and the relationships between LST and land cover indices. This is important because people living in urban areas are vulnerable to the warming climate (Stone et al., 2010). The percent of people living in urban areas was approximately 49 percent of the World's population in 2005, but is expected to increase to approximately 66 percent by 2050 (United Nations, 2014). As

carbon dioxide levels increase, (IPCC, 2013) from anthropogenic emission, contrasting heat stress in urban and rural areas increases (Fischer et al., 2012, Grundstein & Dowd, 2011). Along with increases in heat stress, there have been notable increases in EHEs (Stone et al., 2010; Grundstein & Dowd, 2011; Sheridan & Dixon, 2016). Coupled, EHEs and heat stress within the SUHI are of importance due to morbidity and mortality that has been associated with these events (CDC, 2006; Rey et al., 2007; Luber & McGeehin, 2008; Robine et al., 2008; Romero-Lankao et al, 2012). Furthermore, scholars note that these events also disproportionately affect minorities, older and younger people, people with low education, and low-income people (Harlan et al. 2008; Huang et al., 2011; Uejio, 2011; Romero-Lankao & Dickinson, 2012; Heusinkveld et al., 2014; Pearsall, 2017). In addition to these groups being sensitive to the SUHI, they lack the ability to cope with EHEs, increasing rates of mortality (Buechley et al., 1972; Anderson & Bell, 2011).

2.6 Chapter 2 Tables

Table 2.1: Examples of the variables expressed in equation 1 of the surface energy balance (Rizwan et al., 2007).

Variable	Example
Q^*	Total short wave and long wave radiation emitted absorbed received or diffused in an area.
Q_F	Heat released from humans (factory, cars, etc.)
Q_H	Outdoor air temperature and skin contact
Q_E	Evaporation from vegetation
ΔQ_s	Total heat stored in all built-up materials, vegetation, etc.
ΔQ_A	Change in air mass (advection)

Table 2.2 Sample of satellites and their thermal bands used in quantifying the SUHI.

Satellite	Thermal Wavelengths
Landsat Series	10.40 - 12.50
AVHRR	10.5 - 12.5
ASTER	8.13 - 11.65
MODIS	4.4 - 4.5

Chapter Three: Data and Methods

3.1 Study Area

Baltimore City, Maryland, United States is a city located north of Washington, D.C. It is surrounded by Baltimore County, which spans from 39°43'N to 39°11' N and 76° 53' W to 76°21' W. This county and city make up the study area (Figure 3.1). It covers approximately 1,787.19 square kilometers, and it has multiple land covers ranging from rural landscapes to urban cityscapes. These areas are located beside the Chesapeake Bay Estuary, the largest estuary in North America.

3.2 Data Sources

3.2.1 Study Area Shapefile

The American Community Survey (ACS) block groups for Maryland were imported into ArcMap. The Block Group GEOID for Baltimore County and Baltimore City were selected using the attribute selection tool. The selected data were exported as a shapefile. This shapefile was dissolved to create an outline polygon of the study area. Baltimore City and Baltimore County block group data were then selected individually and exported as separate shapefiles. These were dissolved and used throughout analyses.

3.2.2 Precipitation Data

Similar to other studies (Table 2.1), all satellite images for this study need to be similar and adhere to the following criteria: same time of day; same season; ≤ 10 percent cloud cover. Unlike previous studies, preceding precipitation, specifically rain, must be a selection criterion in this study. Four images of the study area without any precipitation within the previous three days, along with four images of the study area with precipitation within the previous three days, were selected for analysis. Only the three

days before the images were examined for precipitation because most surface water will likely have evaporated over that period; using only one or two days before the images reduced the available images.

Precipitation data from the Global Historical Climatological Network (GHCN) were compared with the dates of acquisition of the satellite images. Two weather stations were used from the GHCN; these were chosen because of the relocation of the weather station from the Baltimore Science Center to the Baltimore Washington International Airport. GHCN data are from the Baltimore-Washington International Airport from May 1, 1970 to May 31, 1999 and from the Baltimore Science Center from May 1, 1998 to April 28, 2017.

3.2.3 Satellite Imagery

The Landsat series of Earth observing satellites were selected for this analysis because of their moderate resolution, spectral characteristics, long period of record, and spatial extent, which has been shown to be sufficient in studies of the SUHI (Deng & Wu, 2013; Roy et al., 2014; Rivera et al., 2017). Eight Landsat satellite images of Baltimore, Maryland were amassed from Earth Explorer at the URL www.earthexplorer.usgs.gov/ with the Worldwide Reference System (WRS) notation path 15, row 32 and path 15, row 33. The acquisition years of the images span the 1990-2016 period and were captured by Landsat 5 Thematic Mapper (TM) and Landsat 8 Operational Land Imager (OLI) and Thermal Infrared Sensor (TIRS). Landsat 5's bands one to five are thirty-meter resolution. The thermal band is 120-meter resolution at capture but is resampled to thirty-meter resolution. Landsat 8's bands one to five are thirty-meter resolution. The thermal

band, band ten, is one hundred-meter resolution at capture but resampled to thirty-meter resolution.

Landsat 5 images were found searching both path 15, row 33 and path 15, row 32. Landsat 5 scenes were then mosaiced and clipped to the study area shapefile. Landsat 8 scenes were found searching path 15, row 33. Landsat 8 scenes cover a larger area than Landsat 5 and they did not require mosaicing. These eight scenes are Collection 1 Level-1 scenes (Table 3.1). Collection 1 Level-1 scenes are a Tier 1 product from the USGS. Tier 1 images have the highest data quality and should be utilized for time-series analysis. These satellite scenes are inter-calibrated across different Landsat instruments, corrected radiometrically, and georegistered within recommended tolerances (USGS, 2016).

In order to be consistent across each scene, images were obtained during a summer month (JJA) between 1990 and 2016. Four scenes have preceding precipitation and four scenes have no preceding precipitation. Table 3.1 provides information about all of the selected images. All other variables on Earth Explorer were unchanged (e.g. collection category, sensor identifier, etc.).

3.3 Preprocessing Satellite Scenes

All scenes were converted to a raster within Terrset. This was done by using the Import module, which reads the MTL file of a scene. Multispectral bands were then converted to reflectance and corrected using Dark-object subtraction. The thermal bands were imported and keep their raw digital numbers.

3.3.1 Landsat 5 Scenes

All Landsat 5 scenes were mosaiced together before being clipped to the study area boundary. Using TerrSet's Mosaic module, each band from path 15, row 33 and path 15, row 32, were mosaiced together. This allowed for the capture of the entire study area. The study area shapefile was then imported from ArcMap into TerrSet. Using the Reformat module, the shapefile from ArcMap was converted to a raster, and all the pixels within the polygon of the study area were assigned a value of a 1, everything outside of the polygon was assigned a value of 0. This raster was then multiplied over every band, using the Overlay module, First * Second. This allowed for all bands to be clipped to the combined Baltimore County and City shapefile.

3.3.2 Landsat 8 Scenes

Each Landsat 8 scene's bands, from path 15, row 33, were imported into TerrSet. The study area shapefile was then imported from ArcMap into TerrSet. This had to be reformatted from a vector to a raster file in order to clip the study area. This was completed using the Reformat module in terrset. Using the Reformat module, the shapefile was converted to a raster and all the pixels within the polygon of the study area were assigned a value of a 1, everything outside of the polygon was assigned a value of 0. This raster was then multiplied over every band, using the Overlay module, First * Second. This allowed for all bands to be clipped to the combined Baltimore County and City shapefile. LST was then calculated as discussed in section 3.4.

3.4 Land Surface Temperature Retrieval

LST retrieval was completed with TerrSet Geospatial Monitoring and Modeling System. The following steps show the workflow for deriving the LST from Landsat 5 and Landsat 8 scenes. Steps are listed in Figure 3.2.

3.2.1 NDVI

NDVI was calculated using the Overlay module in Terrset. NDVI is computed as follows:

$$NDVI = \frac{NIR-Red}{NIR+Red} \quad (2)$$

Landsat 5 band designation for NIR is band 4 and for Red is band 3; Landsat 8 band designation for NIR is band 5 and for Red is band 4. These bands were used in equation 2 and NDVI was calculated for all eight images.

3.2.2 Emissivity

The thermal function in TerrSet calculates blackbody temperatures. Land surfaces are not black bodies but gray bodies (Becker & Li, 1990); Emissivity, therefore, must be considered. NDVI has been used in the reclassification of emissivity (Liu & Zhang, 2011; Ngie et. al., 2014; Alghamdi & Moore, 2015) therefore, NDVI was calculated. An Idrisi Macro Language (IML) script was used to calculate emissivity. Figure 3.3 shows the IML file for the calculation.

3.2.3 Thermal Function

The thermal module in TerrSet was used to calculate LST. For Landsat 8 scenes, the offset, gain, K1, and K2 values (found in the MTL file) of each satellite image were input where it was labeled offset, gain, K1, and K2. The default input background value

and output background value are kept at 0. The wavelength for the thermal band was changed from 11.5 to 10.895. The dialog box, Figure 3.4, shows prompts for the values as well as adding the emissivity file and thermal band 10. For Landsat 5 scenes the wavelength will stay at 11.5 μm and all defaults are kept the same. LST will then be calculated and corrected for emissivity, as noted in 3.2.2, by using the Thermal Function module.

Two equations are used in this module to calculate LST. The first converts digital numbers (DN) to LST. This was created by Bartolucci and Chang (1988). The process takes the DNs from Landsat 5 scenes and converts them to black body temperature by converting DNs to a band specific, pre-specified spectral radiance, and then converting the radiance to a blackbody temperature.

Following the calculation of the blackbody temperature, emissivity must be corrected so that LST represents the correct amount of radiance coming from the surface. This is completed using equation (Eastman, 2016):

Where,

$$S_t = \frac{T_B}{1 + (\lambda x T_B / \rho) x \ln \epsilon} \quad (3)$$

S_t is the surface temperature, T_B is the black body temperature (calculated above), λ is the wavelength of emitted radiance in micrometers, ρ is equal to $h \times (c / \sigma) = 1.438 \times 10^{-2}$ (mK), σ is the Boltzmann constant (1.38×10^{-23} J / K), h is Planck's constant (6.626×10^{-34} Js), c is the velocity of light (2.998×10^8 m/s), and ϵ is the emissivity in the range (0.0, 1.0).

3.5 SUHI Analysis

Multiple analyses were performed on the eight images to address the three research questions:

- 1) Does preceding precipitation influence the magnitude of Baltimore's SUHI?
- 2) Does preceding precipitation influence the clustering of micro SUHIs in Baltimore?
- 3) Does preceding precipitation influence the relationships between LST, NDVI, NDBI, NDWI in Baltimore?

3.5.1 Does preceding precipitation influence the magnitude of Baltimore's SUHI?

Research question 1 was addressed two different ways. The first involved comparing LST inside of the Baltimore City boundary with LST outside of the city boundary. The second involved comparing the LST of urban pixels to the LST of non-urban pixels.

Raw LSTs were aggregated to the Baltimore City and Baltimore County (minus Baltimore City) boundaries. These two regions represent urban and rural, respectively. Mean LST was calculated for these two regions and used to estimate the magnitude of Baltimore's SUHI with:

$$SUHI\ Magnitude = \text{Urban mean temperature (raw)} - \text{rural mean temperature (raw)} \quad (4)$$

For the second method, the land cover of the images was classified using an unsupervised approach and the Anderson Classification. These were implemented in the TerrSet module CLUSTER. Land cover was classified by pixel into six categories: 1) Urban or built-up land, 2) agricultural land, 3) forest land, 4) water, 5) wetland, and 6) barren land. The RECLASS module was used to reclassify pixels in the urban and built-

up land to a 1 to represent urban pixels. All other pixels were classified with a 2 to represent non-urban pixels. Figure 3.5 shows one of the completed unsupervised classifications. Equation 5 was used to quantify the SUHI magnitude as the difference between the mean LST of the urban and non-urban pixels.

3.5.2 Does preceding precipitation influence the clustering of micro SUHIs in Baltimore?

Research question 2 was addressed using the Getis-Ord Gi* cluster analysis on raw LST. This statistic was used to identify clusters of high and low LST within the SUHI, and to determine if LST clusters differently with and without preceding precipitation. The Getis-Ord Gi* statistic cannot be run on raster data, therefore the LST rasters for each image were converted to points using the Create Fishnet (Data Management) tool. Before this could be done, the LST rasters that were converted in TerrSet had to be masked to the study area to ensure there were no outside-of-study-area pixels being converted. Cell width and cell height were set to 30 m to match the resolution of the Landsat scenes. Geometry type was set to polygon and all other options were kept default.

The fishnet produced two shapefiles. These include a labels shapefile and a points shapefile. The labels shapefile was combined with the masked LST raster using the Extract Values to Points tool. The fishnet had to be clipped to the LST mask again to remove points outside of the study area boundary. The clipped and updated values to points shapefile was used as the input into the Hot Spot Analysis (Getis-Ord Gi*) tool. For visualization, the results of the Hot Spot Analysis were interpolated to a raster with the inverse distance weight (IDW) approach, which created a continuous surface of clustered hot and cool surfaces.

3.5.3 Does preceding precipitation influence the relationships between LST, NDVI, NDBI, NDWI in Baltimore?

Research question 3 was addressed by visually comparing and using linear regression to analyze the relationships between LST and NDVI, NDBI, and NDWI. The derivation of NDVI is provided in section 3.2.1.

NDWI and NDBI have been used in SUHI studies (McFeeters, 1996; Zhang et al., 2009) NDWI has been used to demarcate and enhance open-water features. It is possible that NDWI changes when preceding precipitation occurs. NDWI is different depending on land cover. NDBI has been used to show built-up areas and is often used to study the association between SUHIs and LC (Sun et al., 2012). These were calculated using the OVERLAY module in TerrSet. NDWI and NDBI are calculated as:

$$NDWI = \frac{\text{Green} - \text{NIR}}{\text{Green} + \text{NIR}} \quad (5)$$

$$NDBI = \frac{\text{SWIR} - \text{NIR}}{\text{SWIR} + \text{NIR}} \quad (6)$$

The linear regressions were performed with the Regress module within TerrSet, with LST set as the dependent variable and the LC indices set as the independent variables. Figure 3.6 shows the Regress Module. When calculating the regression you must use a boolean mask to ensure that pixels within the study area are analyzed. If the mask is not used it will account for pixels outside of the study area that are 0. This would affect the regression analysis. These were analyzed in ArcMap and extracted by mask to the study area rasters.

Finally, a transect was created. This transect can be seen in Figure 3.7. It extends from Gwynns Falls to Druid Park and southeast past Patterson Park toward the Bay. This transect was created using the 3D Analyst in ArcMap. Transects were also created for NDBI, NDVI, and NDWI.

3.7 Chapter 3 Figures

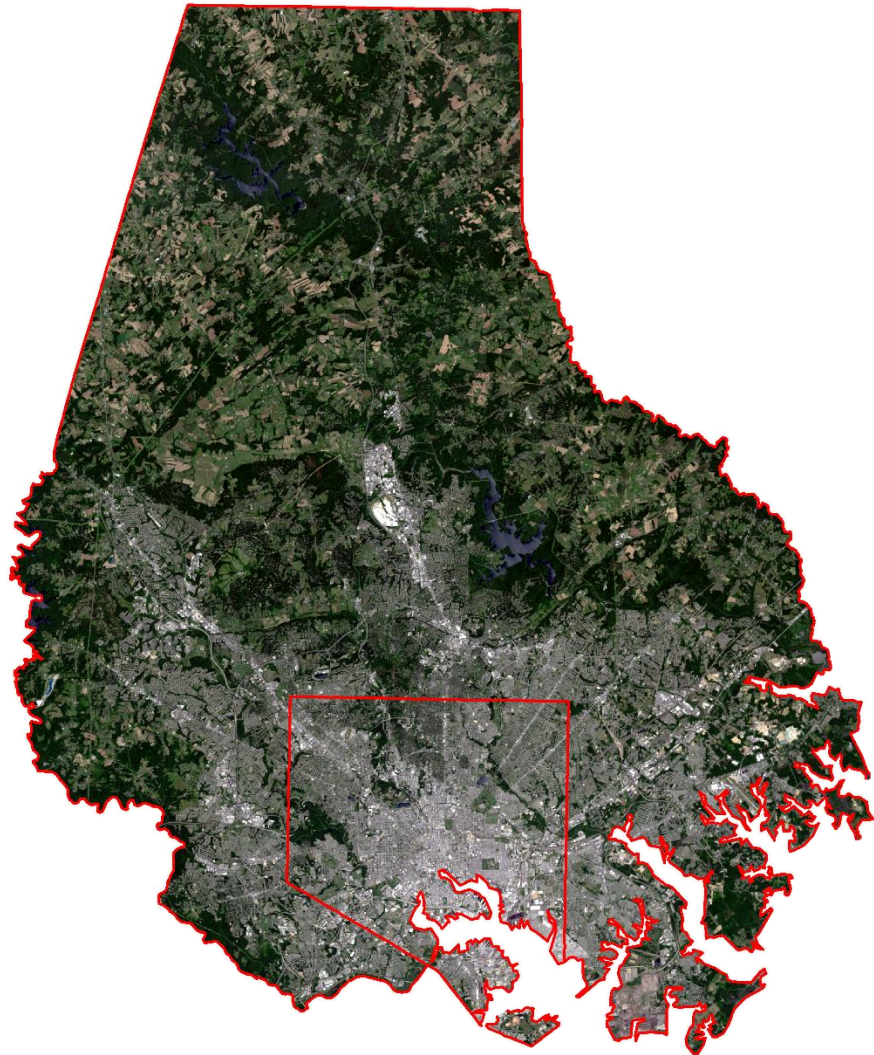


Figure 3.1. Study area color composite with Baltimore County and City combined polygons for the study area.

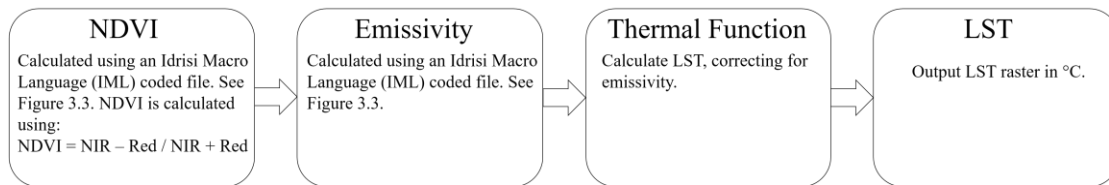


Figure 3.2 represents the process for calculating LST for a specific area.

```

File Edit Tools Help
vegindex x 2*x11ndvi*win_band4*win_band5
display x a*x11ndvi*ndvi*y
reclass x i*x11ndvi*x11temp1*2*0.995*-1.000*-0.185*0*-0.185*1.000*-9999*2
display x a*x11temp1*quant*y
reclass x i*x11ndvi*x11temp2*2*0*-1.000*-0.185*0.970*-0.185*0.157*0*0.157*1.000*-9999*2
display x a*x11temp2*quant*y
reclass x i*x11ndvi*x11temp3*2*0*-1.000*0.727*0.990*0.727*1.000*-9999*2
display x a*x11temp3*quant*y
reclass x i*x11ndvi*x11temp4*2*0*-1.000*0.157*0*0.727*1.000*-9999*2
display x a*x11temp4*quant*y
reclass x i*x11temp4*x11temp5*2*0*0*0.00001*1*0.00001*1.000*-9999*1
display x a*x11temp5*quant*y
transform x x11temp4*x11temp6a*2
display x a*x11temp6a*quant*y
scalar x x11temp6a*x11temp6b*3*0.047
display x a*x11temp6b*quant*y
scalar x x11temp6b*x11temp6c*1*1.0094
display x a*x11temp6c*quant*y
overlay x 3*x11temp5*x11temp6c*x11temp7
display x a*x11temp7*quant*y
overlay x 7*x11temp1*x11temp2*x11temp1
display x a*x11temp1*quant*y
overlay x 7*x11temp3*x11temp1*x11temp2
display x a*x11temp7*quant*y
overlay x 7*x11temp7*x11temp2*x11emissivity
display x a*x11emissivity*quant*y

```

Figure 3.3 is the Idrisi Macro Language (IML) code used to calculate NDVI and emissivity.

The image shows a software dialog box titled "THERMAL- thermal to blackbody conversion". It contains several input fields and radio buttons for configuring the thermal conversion process. The fields include "Thermal band", "Output temperature band", "Wavelength", "Default input background value", "Output background value", "Offset", "Gain", "K1", and "K2". There are also radio buttons for "Data source" (Landsat 4, Landsat 5, Other) and "Calculate temperatures in" (degrees Celsius, degrees Kelvin, degrees Fahrenheit). A checkbox labeled "Correct for emissivity" is present, with an "Emissivity band" field next to it. The dialog box has "OK", "Close", and "Help" buttons at the bottom.

THERMAL- thermal to blackbody conversion

Thermal band :

Output temperature band :

Data source

☐ Landsat 4 ☐ Landsat 5 ☒ Other

Calculate temperatures in

☐ degrees Celsius ☐ degrees Kelvin ☒ degrees Fahrenheit

☐ Correct for emissivity : Wavelength :

Emissivity band :

Default input background value : Output background value :

Offset : Gain : K1 : K2 :

OK Close Help

Figure 3.4 shows the prompts used to run the thermal conversion module. Areas to correct for emissivity and add in the thermal band are shown above.

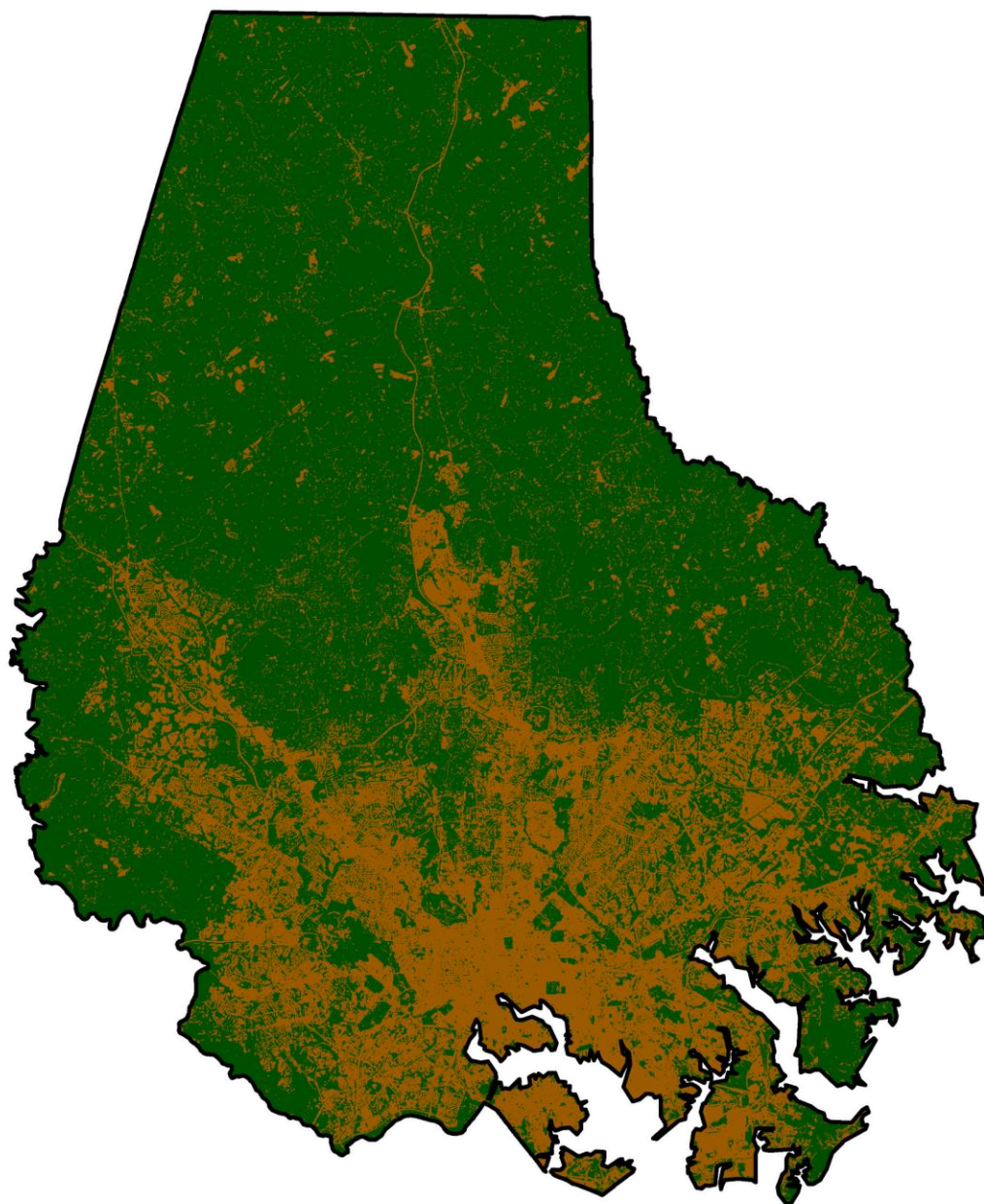


Figure 3.5 Reclassification of urban and non-urban pixels for 2 July 2016 using the CLUSTER module. Green are the non-urban pixels. Light brown are the urban pixels.

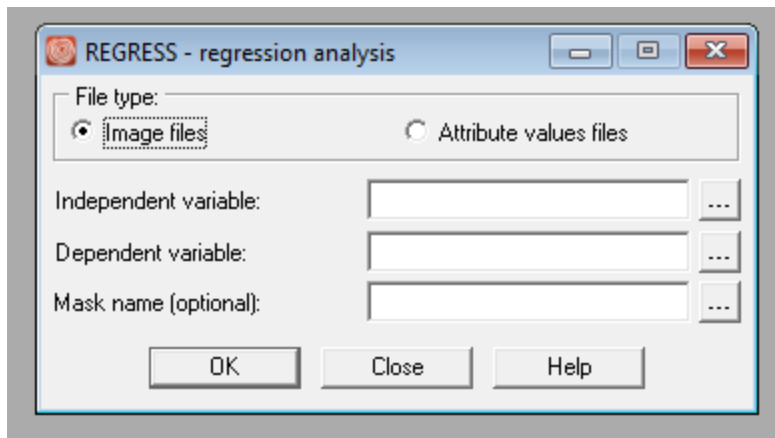


Figure 3.6 shows the Regress module for calculating the linear regression for NDVI, NDBI, NDWI, and LST.

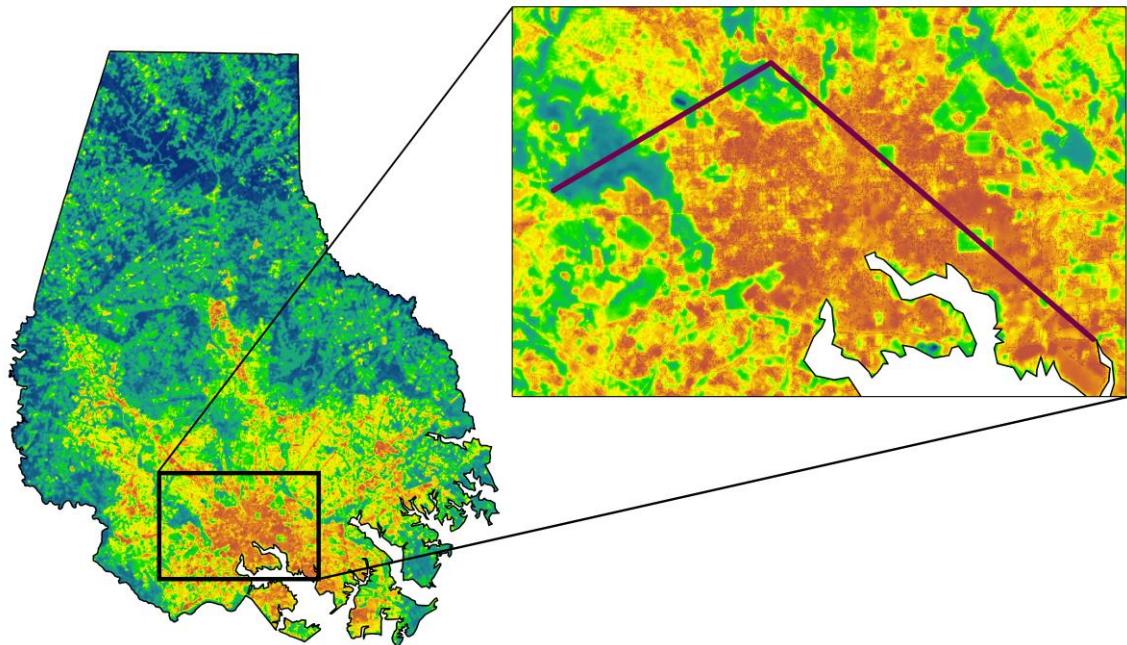


Figure 3.7. LST transect location, 2 July 2016. The transect extends from Gwynns Falls to Patterson Park and southeast toward the Chesapeake Bay.

Chapter Four: Results

Results of the analysis of the influence of preceding precipitation on Baltimore's SUHI are presented herein. It is important to note when reviewing these results that the intent is not to compare individual images but rather to compare statistics for satellite images with preceding precipitation and with no preceding precipitation (Tables 4.1, 4.2, 4.3, 4.4, 4.5, 4.6 and Figures 4.1, 4.2, 4.3, 4.4, 4.5, 4.6). For example, when viewing NDVI in Table 4.4, the intent is to compare the average NDVI of 0.59 with preceding precipitation to the average NDVI of 0.60 without preceding precipitation rather than comparing the average NDVI on 17 August 2015 to 2 July 2016.

4.1 Overview of Baltimore's SUHI

Figure 4.1 shows the LST throughout the city and county of Baltimore for all Landsat images. LST increased toward the center of Baltimore City and decreased in Baltimore County. Arterial roadways extend outward from the center of Baltimore City and appear as extensions of higher LST. For instance, smaller built-up areas around Towson, Maryland are orange colored or warmer LST. As you move East and West from this roadway, LST cool and colors range from blue to green.

Table 4.1 has the statistics for all calculated LST. Days with no precipitation saw an average LST that was greater than scenes with preceding precipitation. The same pattern was true for minimum LSTs. The maximum LSTs, though, did not follow this pattern and were greater for scenes with preceding precipitation. Days with preceding precipitation had greater variability than days with no precipitation.

As you move toward the northern area of Baltimore County, LSTs decrease as agricultural land increases and urban land decreases. Agricultural land can be seen as the

cooler, blue-colored LST. The blue LST includes the water bodies as well. One in particular, the Loch Raven Reservoir, can be seen clearly from the scene dated 9 July 2001 (Figure 4.1 (f) and Figure 4.6 (f)). This reservoir is located just north of Baltimore City and is denoted by a black letter A in each figure.

Transects seen in Figure 4.2 were created for each scene. From 0 to 2,000 m there are low LSTs associated with the Gwynns Falls area. As the transect moves toward Druid Park, LSTs increase as urban cover increases. Druid Park is found around 6,000 m in distance. This is followed by a marked increase in LSTs. At 10,000 m the transect intersects Green Mount Cemetery with a decrease in LSTs followed by an increase. Around 14,000 m, Patterson Park can be seen by the decrease in LST. There is a small increase in LST. This is an area of black top. Following this increase there is once again a decrease in LST.

All transects show decreasing LST for Gwynns Falls, Druid Park, Green Mount Cemetery, and Patterson Park. In Figure 4.2 on 24 August 2006 there is a noticeable decrease in the variability of LST within the city center from 8,000 m to 14,000 m compared to the other images. This decrease in variability is also found in Figure 4.1c. Notice Patterson Park is no longer visible. This occurred on a day where there was no preceding precipitation.

4.2 SUHI Magnitude

The SUHI magnitude statistics are shown in Table 4.2. The County/City method resulted in lower magnitudes than the pixel calculated method. Overall, the greatest difference between the County/City and pixel method was a difference of $\pm 1.6^{\circ}\text{C}$. For instance, there was a 0.74°C difference for the 26 August 2001 scene. This difference

may have been caused by the increased urban and barren surfaces that the pixel method was able to account for. The County/City boundary did not include barren surfaces outside of the city polygon.

For scenes without precipitation, the magnitudes ranged from an average of 4.33 °C to 5.22 °C. Scenes with preceding precipitation had higher average magnitudes than the images without precipitation. Average magnitudes ranged from 4.86 °C to 5.78 °C. In the case of the scenes with preceding precipitation, the greatest difference between magnitudes was about 1.25 °C. This may also be explained by the increase in barren surface being included in the calculation for LST via the pixel method.

4.3 Clustering of LST

The spatial clustering of LST in Baltimore was apparent in every scene. Figure 4.3 shows clustering by confidence interval (CI). Significant clustering of warmer LSTs was consistent in urban areas. Overall, there was little difference in the clustering of high LSTs within the Baltimore City center. LC within Baltimore County experienced areas of significant clustering of warmer LSTs on days with and without preceding precipitation. Three of the scenes had clustering within northern Baltimore County. Two of these occurred on days with no preceding precipitation (Figures 4.3 (b) and (c)) and one with preceding precipitation (Figure 4.3 (g)).

This clustering change in Baltimore County may be due to the LC type. Barren surfaces were found at the location of the small micro clusters of heat. These may be creating small micro heat islands. Looking at Figure 4.3, it should be noted that arterial roadways fell within the 99% statistically significant clustering of LST. This may be useful in deciding the spatial extent of SUHIs.

4.4 Landcover/LST Relationship

NDVI, NDBI, and NDWI can be seen in Figures 4.4, 4.5, and 4.6. Low values of NDVI (Figure 4.4) and NDBI (Figure 4.5) point out urban areas and highlight Baltimore City. NDWI (Figure 4.6) highlights water bodies within the study area. NDBI and NDWI both had on average greater maximums on days with preceding rainfall.

Table 4.3 shows the results of the regression analyses. The average coefficient of determination and R values for NDVI, NDBI, and NDWI were lower for the images with preceding precipitation. The coefficient of determination for NDVI ranged from 49.16 percent to 75.04 percent. The coefficient of determination for NDBI ranged from 52.05 percent to 70.31 percent. The coefficient of determination for NDWI ranged from 41.45 percent to 68.94 percent. NDVI was negatively correlated with LST. NDBI and NDWI were both positively correlated with LST. Images with preceding precipitation had decreased average R values. R values for NDVI and NDBI without precipitation averaged -0.77 and 0.78. R values for images with precipitation ranged from -0.73 to 0.75. NDWI had positive R values in both cases with decreased R values for images with preceding precipitation.

The slope coefficients varied. The average NDVI slope coefficient was -1.28 without preceding precipitation and -1.23 with preceding precipitation. The average NDBI and NDWI slope coefficients were 1.74 without preceding precipitation, 1.85 with preceding precipitation, 1.38 without preceding precipitation and 1.30 with preceding precipitation respectively.

Out of the selected scenes, Landsat 8 images had the highest coefficient of determination and R values in both cases. With preceding precipitation, there was a decrease in the values of the Landsat 8 images. In all cases, NDVI had negative R values

while NDBI and NDWI had positive values. Tables 4.4, 4.5, and 4.6 show a full overview of completed statistics on NDVI, NDBI, and NDWI. There was strong correspondence between these values and LST. Appendix A contains all of the scatter plots from the completed regressions. For transects of NDVI, NDBI, and NDWI see Appendix B.

4.5 Chapter 4 Tables

Table 4.1 LST descriptive statistics. Mean, maximum, minimum, and standard deviation calculated for all scenes.

LST (°C)				
No Rain				
Date	Mean	Max	Min	Standard Deviation
17-Aug-15	29.83	49.76	25.12	3.11
24-Aug-06	25.70	42.44	12.30	3.04
26-Aug-01	23.94	41.64	13.30	2.84
29-Jun-09	26.67	48.76	11.40	3.39
Average	26.54	45.65	15.53	3.10
Rain				
2-Jul-16	28.70	52.04	20.58	4.52
9-Jul-01	27.47	47.66	15.61	2.80
23-Aug-94	21.32	43.15	11.40	2.74
6-Jul-00	24.28	47.25	4.40	3.57
Average	25.44	47.53	13.00	3.41

Table 4.2. SUHI magnitude statistics. Average SUHI magnitudes were greater for images with preceding precipitation.

SUHI Magnitude						
County/City Method (°C)				Pixel Method (°C)		
No Preceding Precipitation						
Date	City	County	Magnitude	Urban	Rural	Magnitude
17-Aug-15	33.79	29.30	4.49	33.34	28.44	4.90
24-Aug-06	29.21	25.22	3.99	29.83	24.24	5.59
26-Aug-01	27.45	23.45	4.00	27.05	22.31	4.74
29-Jun-09	30.95	26.10	4.85	31.05	25.37	5.67
Average			4.33	5.22		
Preceding Precipitation						
Date	City	County	Magnitude	Urban	Rural	Magnitude
2-Jul-16	34.34	27.94	6.40	33.33	26.65	6.68
9-Jul-01	30.29	26.62	3.67	30.82	25.84	4.98
23-Aug-94	25.02	20.82	4.20	25.10	19.95	5.14
6-Jul-00	28.83	23.67	5.16	28.48	22.18	6.30
Average			4.86	5.78		

Table 4.3 Coefficient of determination, R, and slope coefficient values for all selected scenes.

No Preceding Precipitation									
Coefficient of Determination				R			Slope Coefficient (10^{-1})		
Date of Image	NDVI	NDBI	NDWI	NDVI	NDBI	NDWI	NDVI	NDBI	NDWI
17-Aug-15	75.04	70.31	68.94	-0.87	0.84	0.83	-1.45	1.96	1.69
29-Jun-09	51.64	52.05	45.19	-0.72	0.72	0.67	-1.22	1.81	1.31
24-Aug-06	54.68	63.71	41.45	-0.74	0.80	0.64	-1.21	1.65	1.21
26-Aug-01	59.64	58.37	52.15	-0.77	0.76	0.72	-1.26	1.56	1.33
Average	60.25	61.11	51.93	-0.77	0.78	0.72	-1.28	1.74	1.38
Preceding Precipitation									
Date of Image	Coefficient of Determination			R			Slope Coefficient (10^{-1})		
2-Jul-16	58.87	60.32	53.74	-0.77	0.78	0.73	-1.69	2.48	1.89
6-Jul-00	55.53	54.47	47.40	-0.75	0.74	0.69	-1.28	1.83	1.33
9-Jul-01	49.16	53.70	41.56	-0.70	0.73	0.64	-0.97	1.45	0.99
23-Aug-94	49.86	53.89	43.14	-0.71	0.73	0.66	-0.98	1.64	1.00
Average	53.36	55.60	46.46	-0.73	0.75	0.68	-1.23	1.85	1.30

Table 4.4. NDVI descriptive statistics for all images.

NDVI				
No Preceding Precipitation				
Date	Mean	Max	Min	Standard Deviation
17-Aug-15	0.74	0.95	-0.55	0.19
24-Aug-06	0.52	0.83	-0.44	0.19
26-Aug-01	0.55	0.82	-0.38	0.18
29-Jun-09	0.59	0.94	-1.00	0.20
Average	0.60	0.89	-0.59	0.19
Preceding Precipitation				
2-Jul-16	0.59	0.88	-0.71	0.21
9-Jul-01	0.55	0.82	-0.38	0.18
23-Aug-94	0.63	0.94	-0.57	0.20
6-Jul-00	0.60	0.90	-1.00	0.21
Average	0.59	0.89	-0.67	0.20

Table 4.5. NDBI descriptive statistics for all images.

NDBI				
No Preceding Precipitation				
Date	Mean	Max	Min	Standard Deviation
17-Aug-15	-0.28	0.45	-1.00	0.13
24-Aug-06	-0.28	0.51	-1.00	0.15
26-Aug-01	-0.32	0.45	-1.00	0.14
29-Jun-09	-0.32	1.00	-1.00	0.14
Average	-0.30	0.60	-1.00	0.14
Preceding Precipitation				
2-Jul-16	-0.31	0.54	-0.84	0.14
9-Jul-01	-0.35	0.46	-1.00	0.14
23-Aug-94	-0.37	0.64	-1.00	0.12
6-Jul-00	-0.52	1.00	-0.83	0.19
Average	-0.39	0.66	-0.92	0.15

Table 4.6. NDWI descriptive statistics for all images.

NDWI				
No Preceding Precipitation				
Date	Mean	Max	Min	Standard Deviation
17-Aug-15	-0.75	0.63	-0.93	0.15
24-Aug-06	-0.44	0.59	-0.75	0.16
26-Aug-01	-0.48	0.51	-0.74	0.16
29-Jun-09	-0.52	1.00	-0.79	0.18
Average	-0.55	0.68	-0.80	0.16
Preceding Precipitation				
2-Jul-16	-0.57	0.80	-0.78	0.18
9-Jul-01	-0.52	0.77	-0.77	0.18
23-Aug-94	-0.54	0.72	-0.81	0.18
6-Jul-00	-0.52	1.00	-0.83	0.19
Average	-0.54	0.82	-0.80	0.18

4.6 Chapter 4 Figures

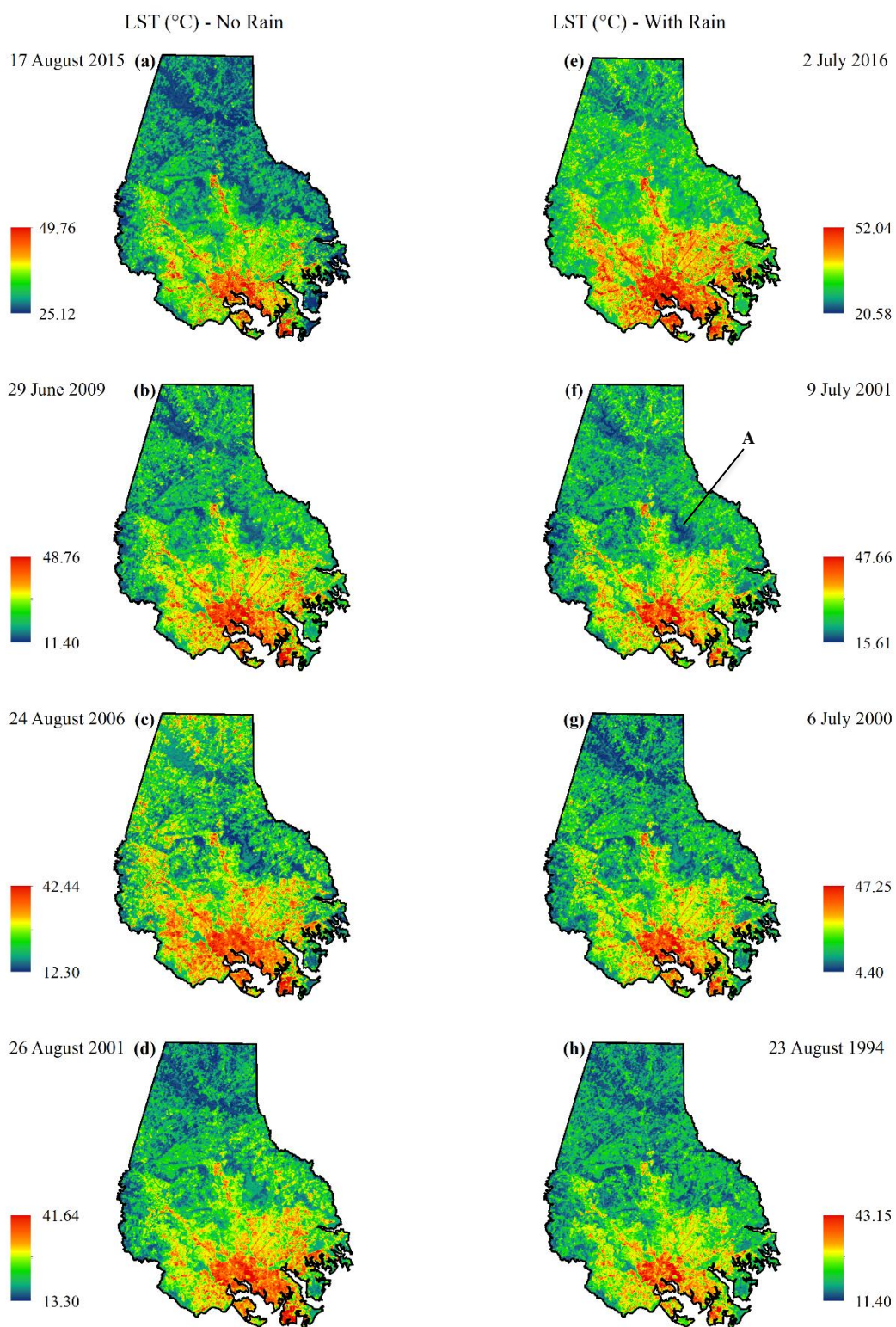


Figure 4.1. LST calculated for all Landsat scenes. Letter A denotes Loch Raven Reservoir.

LST Transects

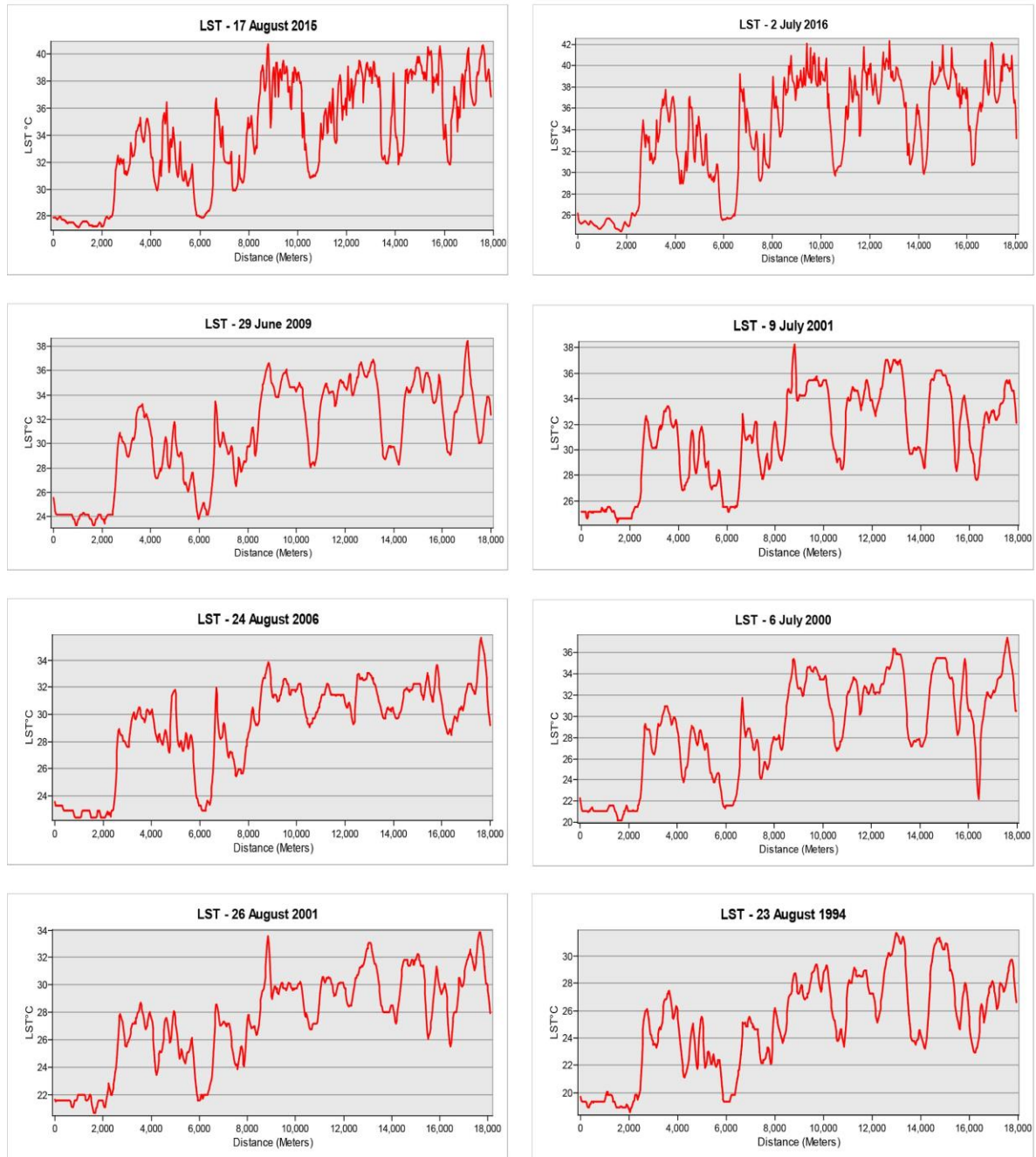


Figure 4.2. LST transects. Each transect runs from Gwynn Falls to Druid Park to Patterson Park and south towards the Bay. See Figure 3.7.

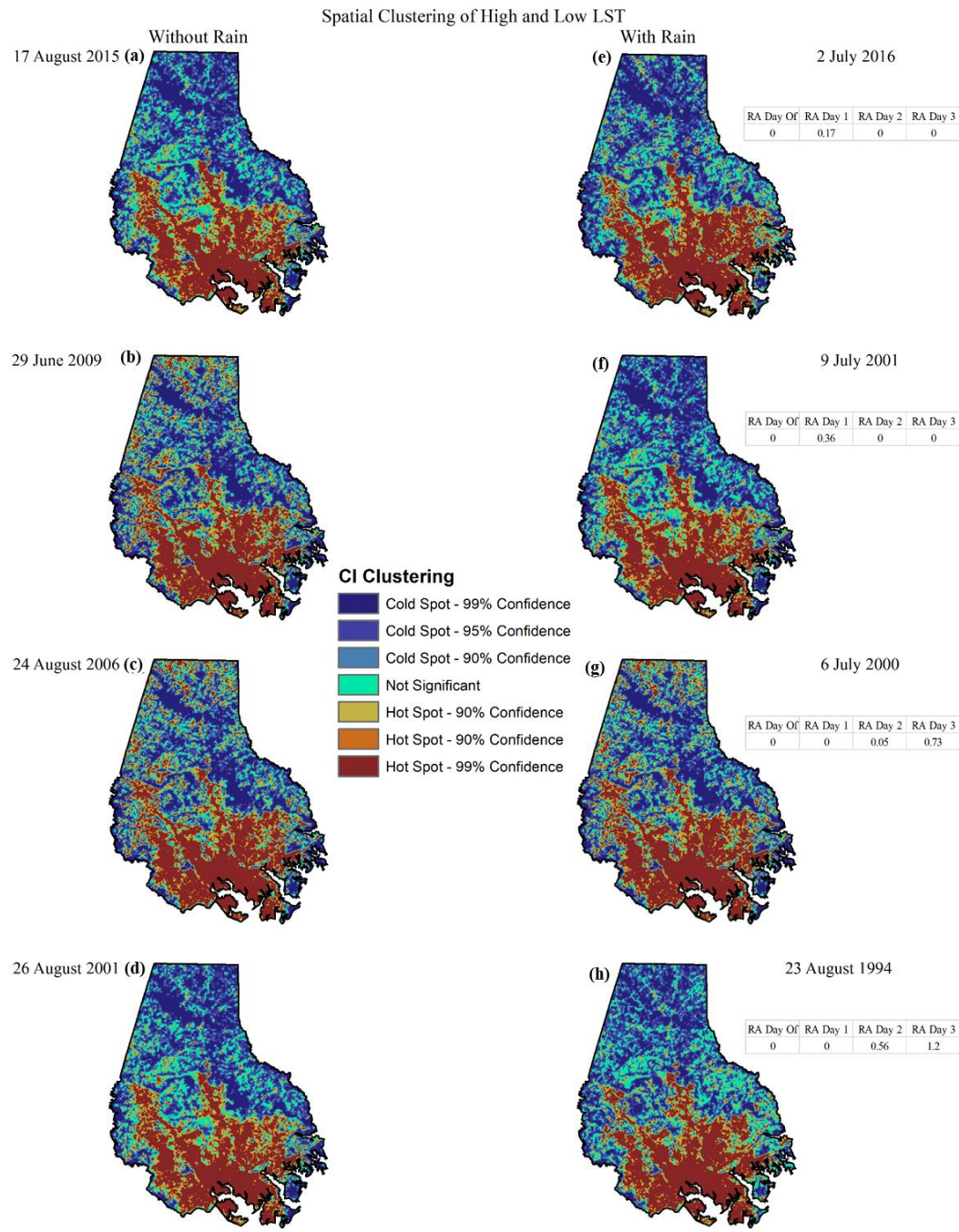


Figure 4.3 Getis-Ord G_i^* spatial clustering statistic shows the confidence intervals (CI) of clustering of high and low LST.

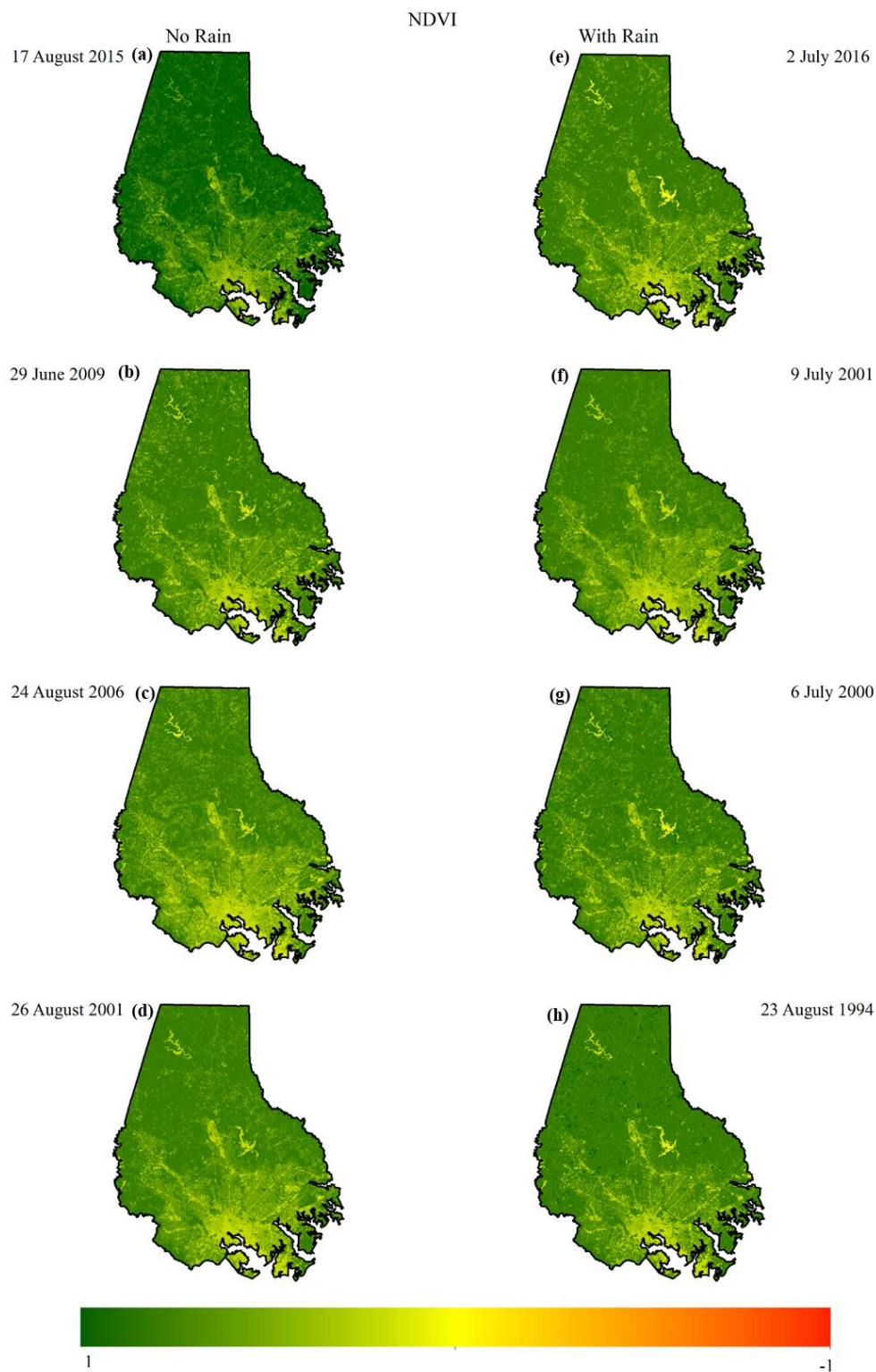


Figure 4.4 Normalized Difference Vegetation Index (NDVI) calculated for all Landsat scenes.

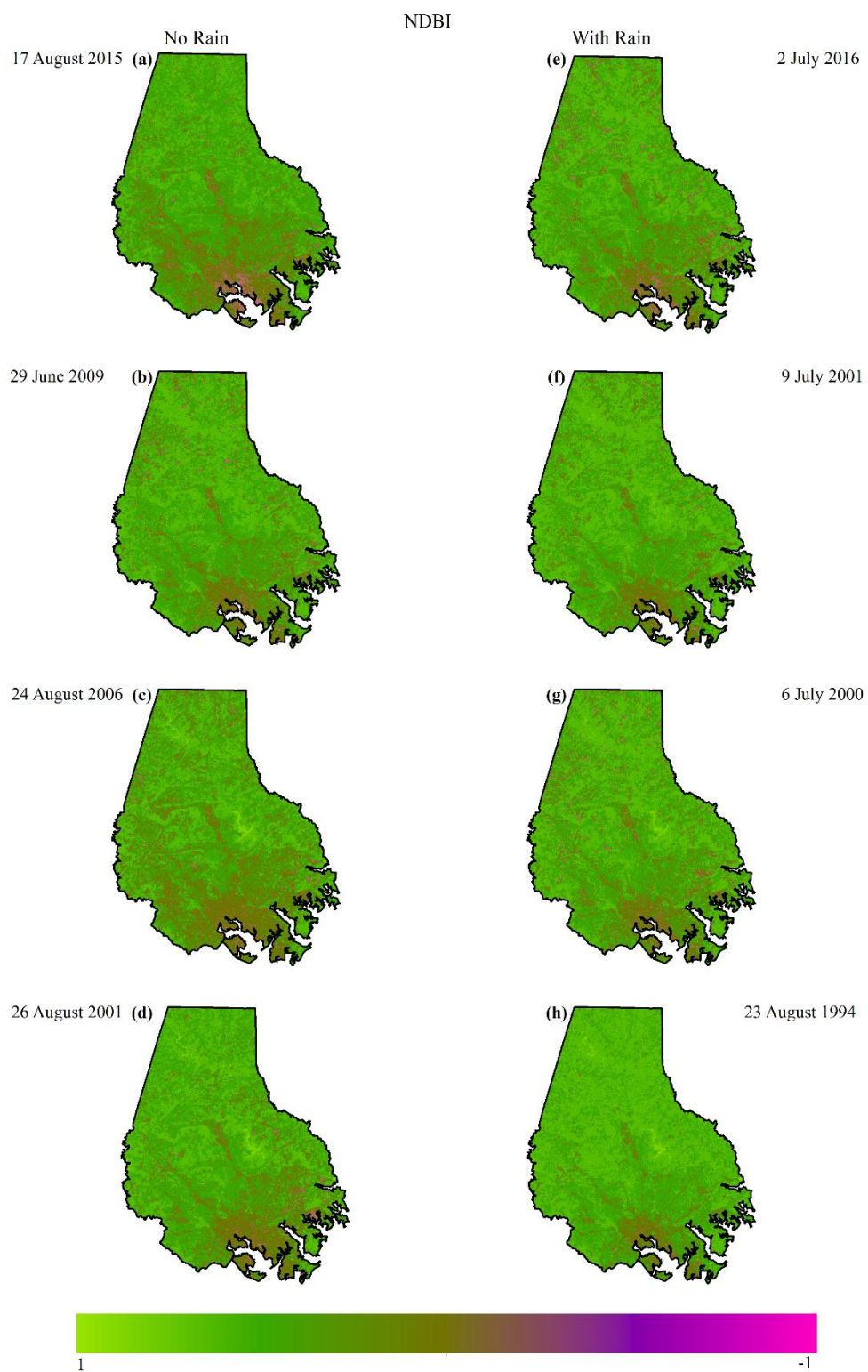


Figure 4.5 Normalized Difference Built-up Index (NDBI) calculated for all Landsat scenes.

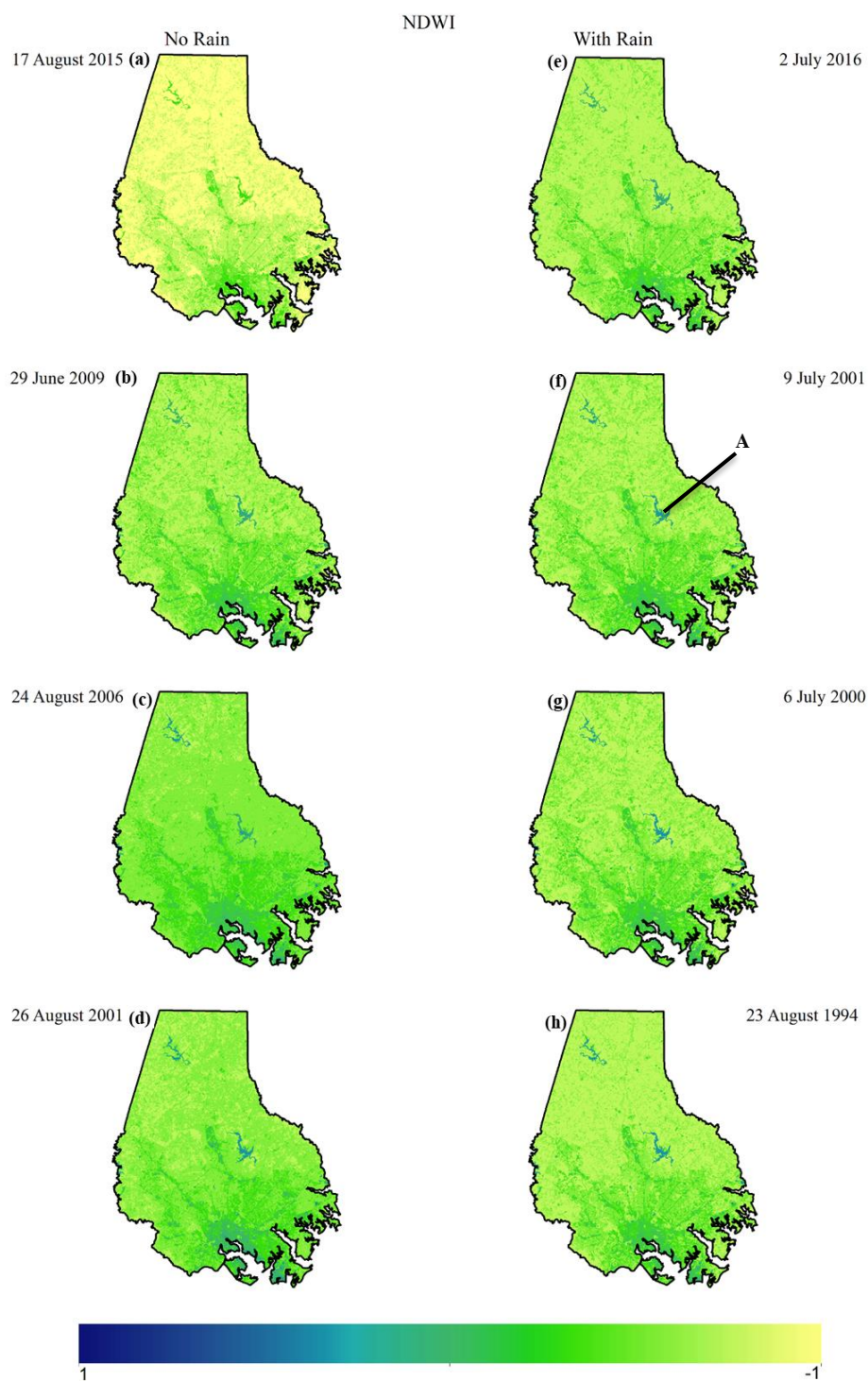


Figure 4.6. Normalized Difference Water Index (NDWI) calculated for all Landsat scenes. The letter A in panel f denotes Loch Raven Reservoir.

Chapter Five: Discussion

5.1 Discussion of Research Questions

SUHIs have been studied since the 1970's using remotely sensed images from different Earth observing satellites. These images are important for temporal and spatial analyses as EHEs are expected to increase in urban areas. These analyses must be done accurately to ensure the correct magnitude of the SUHI is being taken into account. Knowing the impact of preceding precipitation will enhance the accuracy of temporal and spatial SUHI studies and aid in the mitigation of future SUHI.

This thesis aimed to evaluate the effects of preceding precipitation on the remotely sensed SUHI signature. This was completed by addressing the following three questions:

- 1) Does preceding precipitation influence the magnitude of Baltimore's SUHI?
- 2) Does preceding precipitation influence the clustering of micro SUHIs in Baltimore?
- 3) Does preceding precipitation influence the relationships between LST, NDVI, NDBI, NDWI in Baltimore?

For the first question, Baltimore's SUHI magnitude varies between methods. In the case of county/city polygon, the SUHI average was 4.33 °C with no preceding precipitation and 4.86 °C with precipitation. In the case of the pixel method, the average SUHI magnitude was 5.22 °C with no preceding precipitation and 5.78 °C with preceding precipitation.

Overall, when calculating the magnitude of the SUHI within Baltimore, the pixel method used may be a superior method because it accounts for vegetated surfaces within

urban areas and urban surfaces within rural areas. The magnitudes calculated using the classified pixels were greater in most cases. For instance, the arterial roadway extending to the north and including Cockeysville is not included when using the administrative county/city polygon method. Unfortunately, the pixel method also tended to classify rural fields with bare soil as urban pixels, especially in images that were unusually warm or dry. It is likely that this mis-classification helped keep the average temperature of Rural pixels lower.

The results presented herein suggest that the SUHI magnitude increases when there is preceding precipitation and decreases when there is no preceding precipitation. This might be a result of urban, impervious surfaces warming quicker than vegetated surfaces after the precipitation, causing the magnitude to increase. The magnitude may also be influenced by the time since precipitation, the duration of precipitation, and the amount of precipitation. These possible influences should be explored using a controlled experimental design.

For the second question, the Getis-Ord G_i^* statistic was inconclusive with regards to isolating the micro SUHIs. It was not able to capture any spatial changes in the variability of the SUHI. Therefore, the clustering within the SUHI was not observed.

There was clustering of higher LST over barren LC. This is thought to be caused by soils and vegetation that lack the ability to absorb or hold water, which allows for quicker drying than the surrounding surfaces. This allows sensible heat to begin building relatively quickly once all surface water has evaporated. These clusters of warmer LST may be considered barren heat islands. These are not the same as barren LC within urban

locales. Instead of being a barren parking lot for instance, it is a location with little to no vegetation and an abundance of soil.

While the Getis-Ord G_i^* statistic did not capture much variability within the SUHI or capture it at a resolution that would allow for differences or similarities to be shown, it did do well showing the extent of the SUHI. There seems to be no consistent method for calculating the extent of the SUHI in the literature. The Getis-Ord G_i^* statistic could be used to objectively outline the extent of the SUHI. For example, the contiguous region of high LST bound by one of the CIs can be used to define the spatial extent of SUHIs.

With regard to question 3, the average coefficient of determination decreased for indices associated with preceding precipitation. Preceding precipitation may lower the explanatory value of these indices. For instance, if a SUHI study was completed using NDVI to aid in the calculation of LST, there may be a reduced reliability and decreased accuracy of the calculated LST.

NDBI and NDWI both showed greater average maximum values on days with preceding rainfall. This might be due in part to the surface water changing the spectral reflectance of wavelengths that are used in the calculation of these indices. For NDWI, mean and minimum values were negative. This is caused by the index highlighting LC such as vegetation and barren surfaces. Vegetation and barren surfaces tend to be negative values and water bodies tend to be positive values.

5.2 Further Research

There was not a detectable difference in the magnitude of the SUHI in Baltimore across the preceding and no preceding satellite scenes. This may be related to days from

the rain event, or the rain event was too small to have a lasting impact. It may also be related to the small number of images collected. To address these limitations, more research should be completed in order to understand the extent of the differences in the changes of the magnitude of the SUHI. Future research might use a different method for classifying urban versus rural land cover and/or different data source such as tax parcel maps or by using a different algorithm. Once the region is classified, the same classification boundaries could be used in all subsequent images. Studies should also collect more satellite imagery to increase sample sizes. Increased sample sizes would allow further analysis to be completed to see if the tendency holds true for preceding precipitation to increase SUHI magnitude. Studies should also include days with greater amounts of precipitation in the antecedent days.

More spatially resolute images should also be utilized in the analysis of the spatial clustering of the SUHI. The Getis-Ord G_i^* statistic should be used on images with greater resolution, for example, the Sentinel satellite series from the ESA has RGB bands at 15 m resolution. The Getis-Ord G_i^* statistic or Hot Spot Analysis should also be used as a method to track changes over time. The spatial extent of the 95th % CI or 99th % CI could be used to demarcate SUHIs. Efforts should focus on contiguous regions of the 95th CI because as shown earlier barren surfaces may have higher LST but are not urban LC. Greater resolution imagery will allow for changes at different spatial scales, for instance, block group to neighborhood scale changes in LST would be useful for the placement of cooling centers.

Additional studies of NDVI and NDBI should be conducted to continue to see if their ability to explain LST decreases with preceding precipitation. NDWI was positively

correlated with LST through the negative portion of the NDWI spectrum, but it is unclear which LCs are represented by different NDWI values. Studies should also include different indices. These studies should look into barren surfaces and impervious surfaces, as well as soil moisture, to see how they affect the clustering of micro SUHIs when preceding rainfall occurs. The addition of these indices would shed light on how preceding rainfall is affecting different LC. Different LC could also be separated to see how every type of land is being affected.

Understanding how preceding precipitation affects the SUHI will help with mitigation purposes such as pavement wetting. Pavement wetting has been completed in Europe and has decreased LST (Hendel et al., 2014). In Baltimore, rainwater can be collected and dispersed over different surfaces, ultimately reducing the LST. Knowing how precipitation affects the UHI phenomena is critical in preventing EHEs and keeping inhabitants of urban areas from reaching LSTs that are unsuitable for human health.

Chapter Six: Summary

This study evaluated the affects that preceding precipitation might have on the remote sensing signature of Baltimore's SUHI. It was guided by three questions:

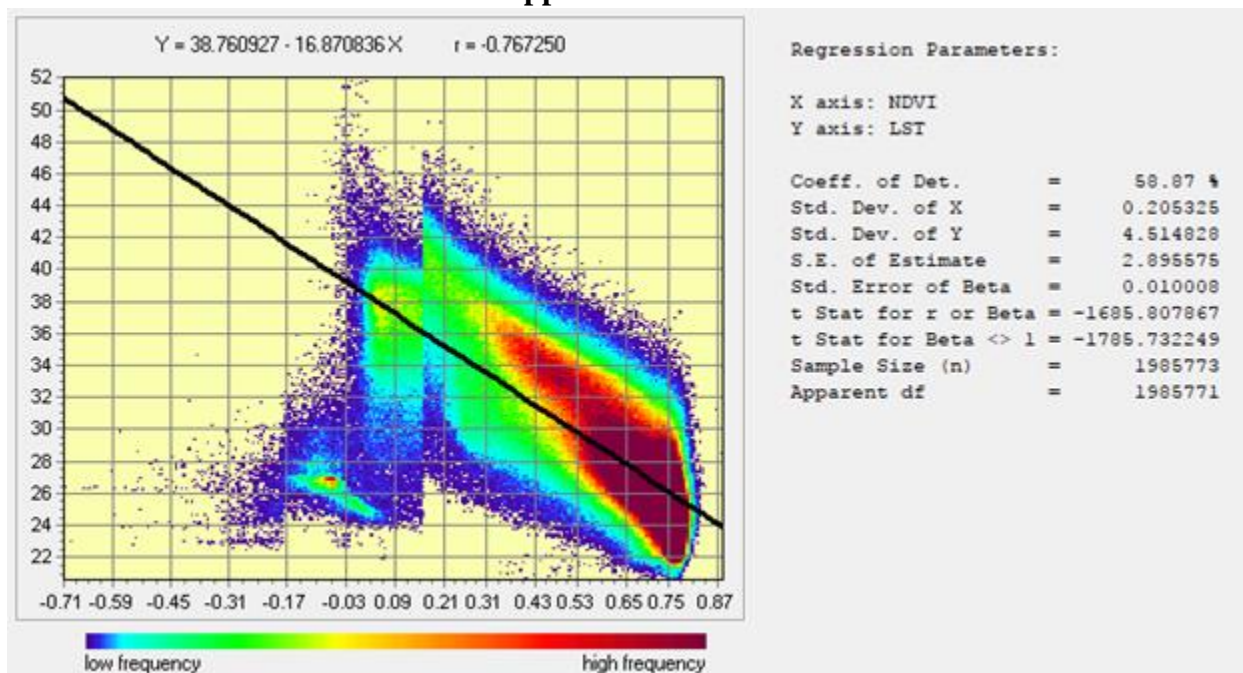
- 1) Does preceding precipitation influence the magnitude of Baltimore's SUHI?
- 2) Does preceding precipitation influence the clustering of micro SUHIs with Baltimore?
- 3) Does preceding precipitation influence the relationships between LST, NDVI, NDBI, and NDWI in Baltimore?

The first question was completed by calculating the magnitude of Baltimore's SUHI with two methods. The first method, the county/city boundaries, on average found that preceding precipitation increased the magnitude of the SUHI in Baltimore. The second method, the unsupervised pixel classification, on average found that preceding precipitation increased the magnitude of the SUHI in Baltimore. The second method of analysis was more accurate in that it included urban pixels that were outside of the city polygon.

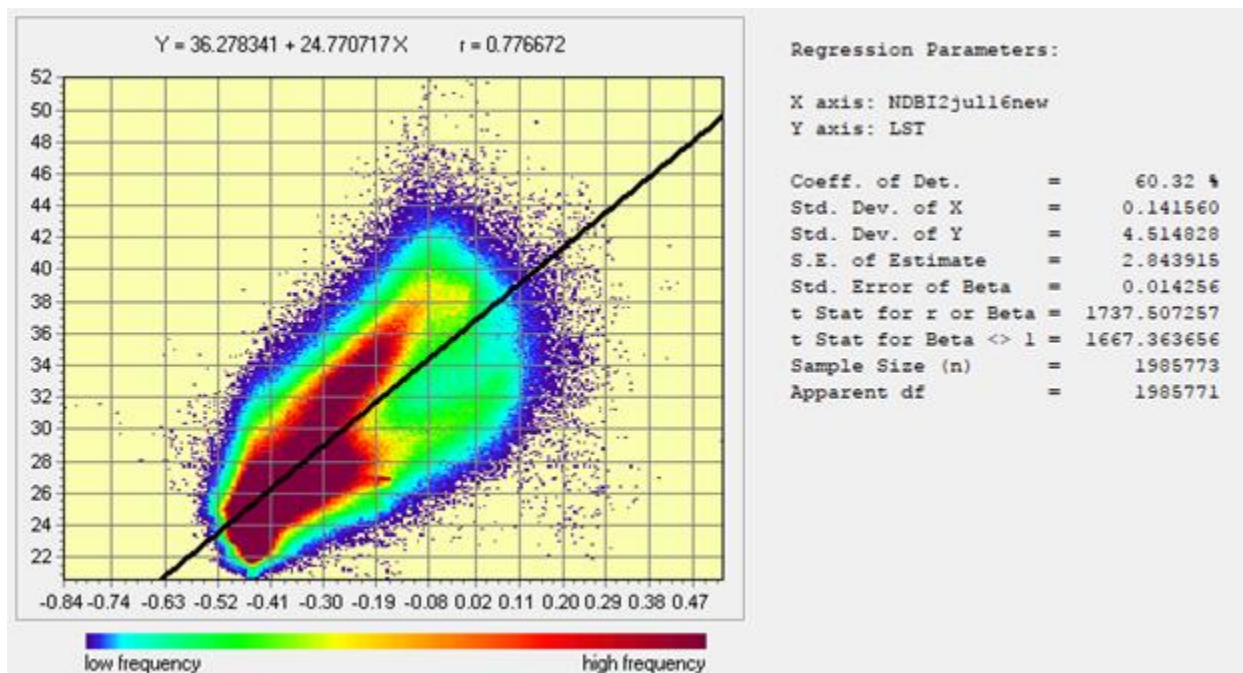
The second question was completed by running the Getis-Ord G_i^* statistic on the calculated LST. Barren fields within Baltimore County had clusters of warmer LSTs. These were noted as barren LC. Overall, the statistic was inconclusive at showing the variability of the clustering of the SUHI. It was useful in delineating an objective extent of the SUHI.

The third question was completed by comparing LST to NDVI, NDBI, and NDWI. This was done by computing a bivariate regression. The relationships between LST and NDVI, NDBI, and NDWI were negative, positive, and positive respectively. This means that as NDVI increases LST decreases, as NDBI increases LST increases, and as NDWI increases LST increases (up to NDWI of 0). NDBI and NDWI had increased maximum values on days with preceding precipitation. Overall, preceding precipitation may affect the explanatory power of the indices.

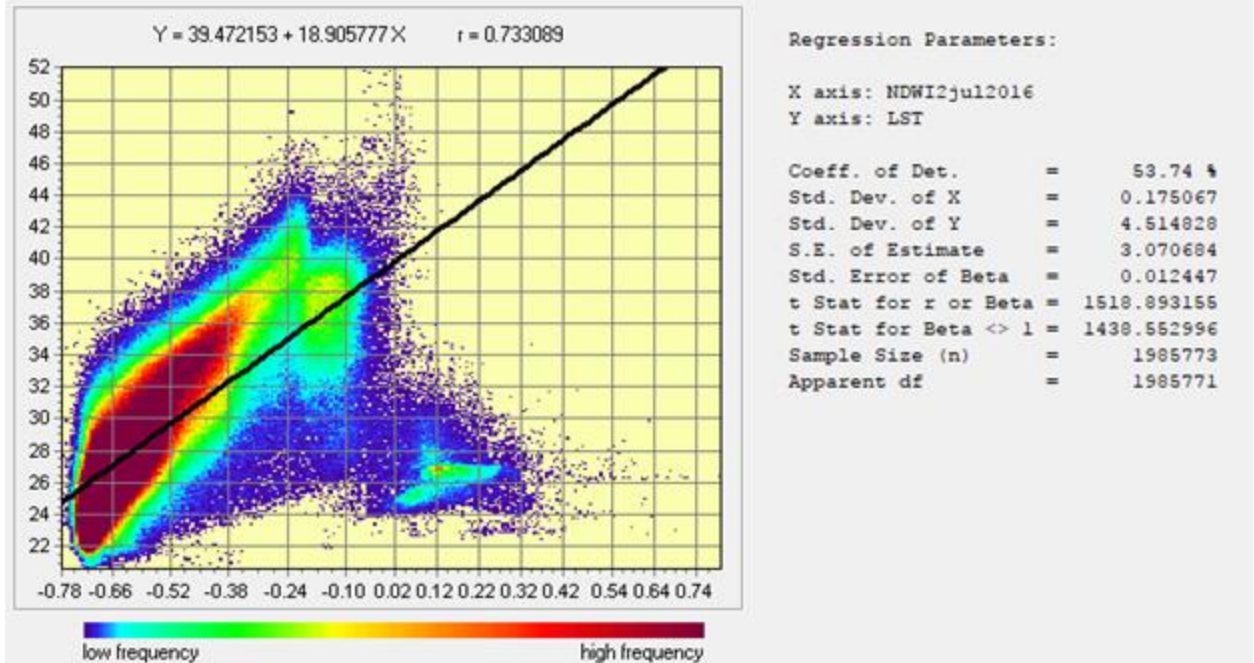
Appendix A



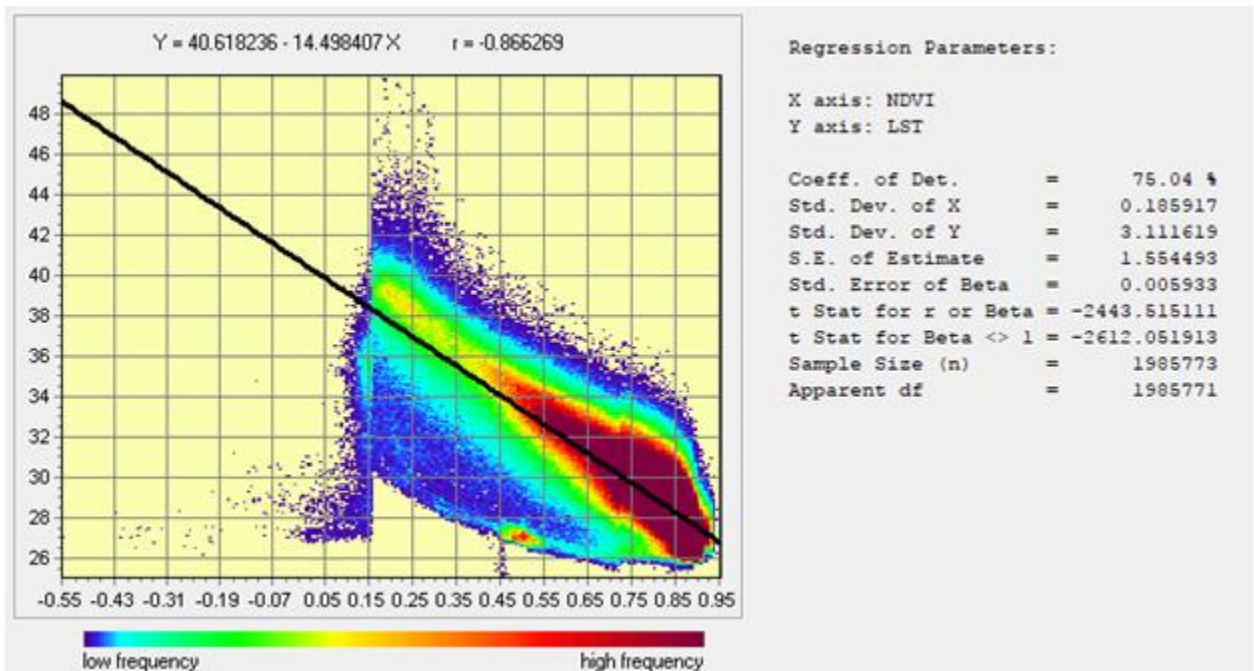
A1. 2 July 2016 - LST regressed on NDVI. Landsat 8 image.



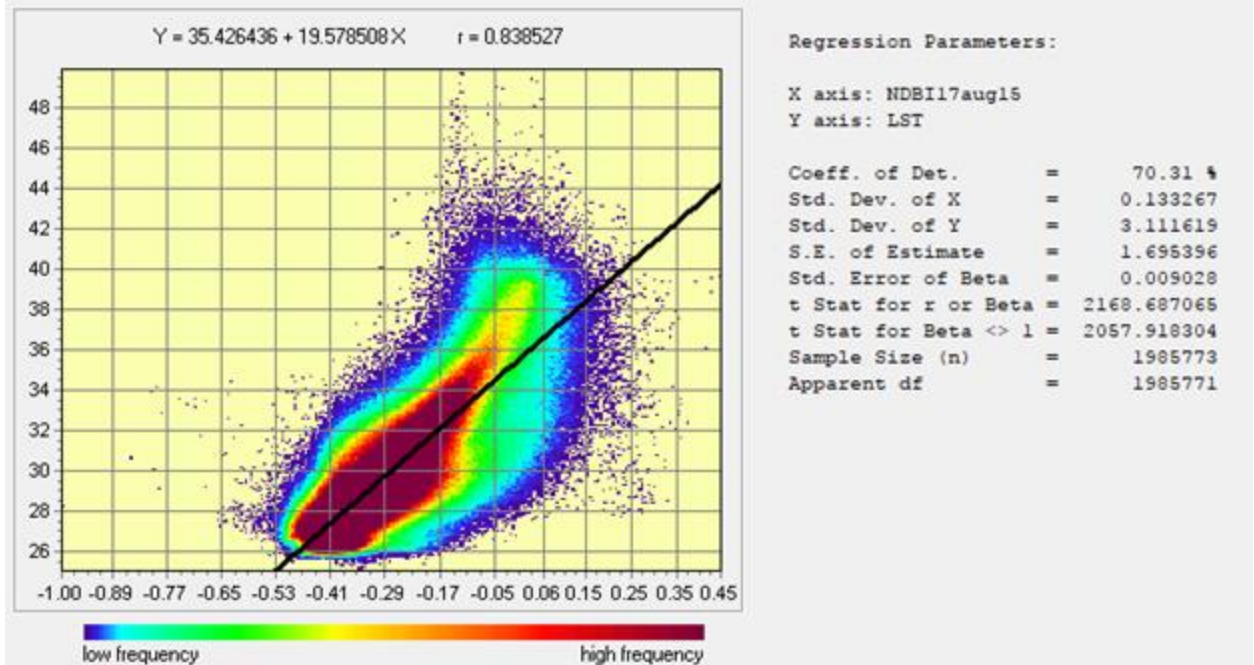
A2. 2 July 2016 - LST regressed on NDBI. Landsat 8 image.



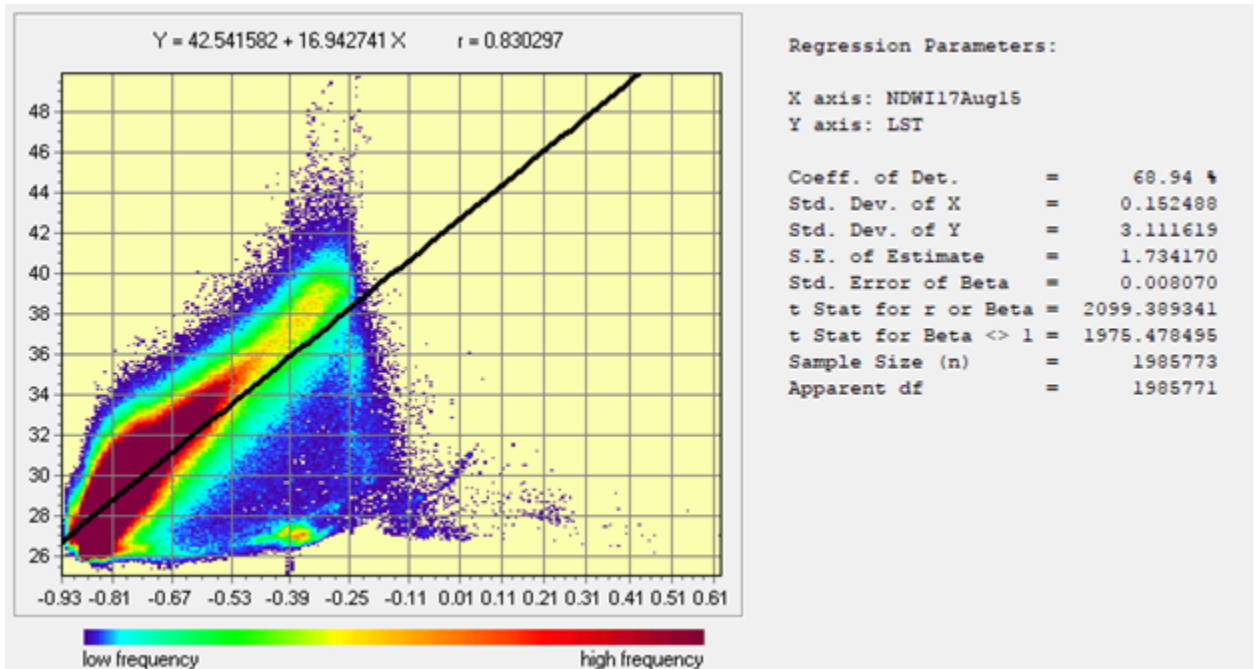
A3. 2 July 2016 - LST regressed on NDWI. Landsat 8 image.



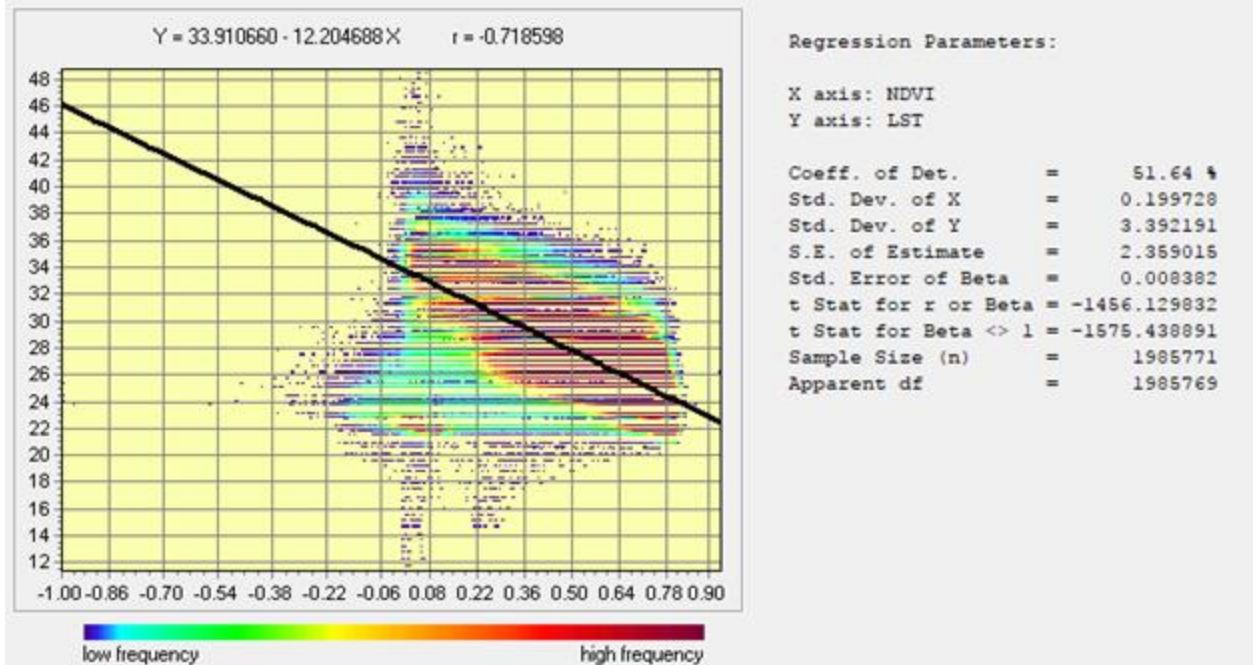
A4. 17 August 2015 - LST regressed on NDVI. Landsat 8 image.



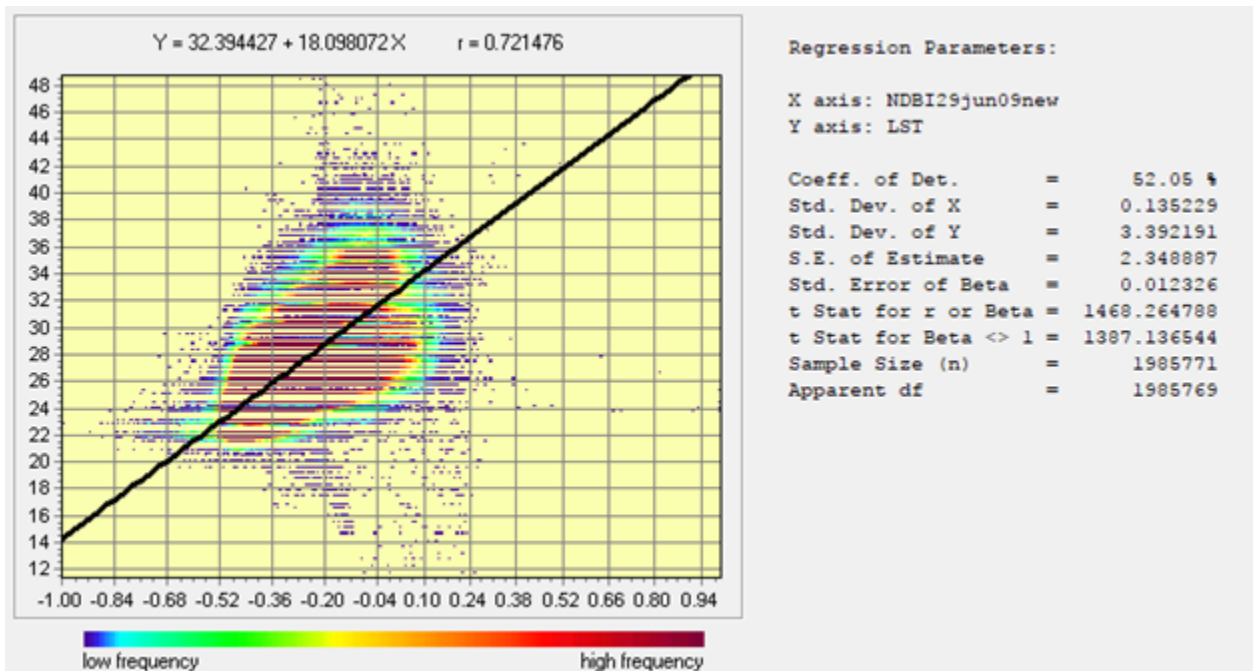
A5. 17 Aug 2015 - LST regressed on NDBI. Landsat 8 image.



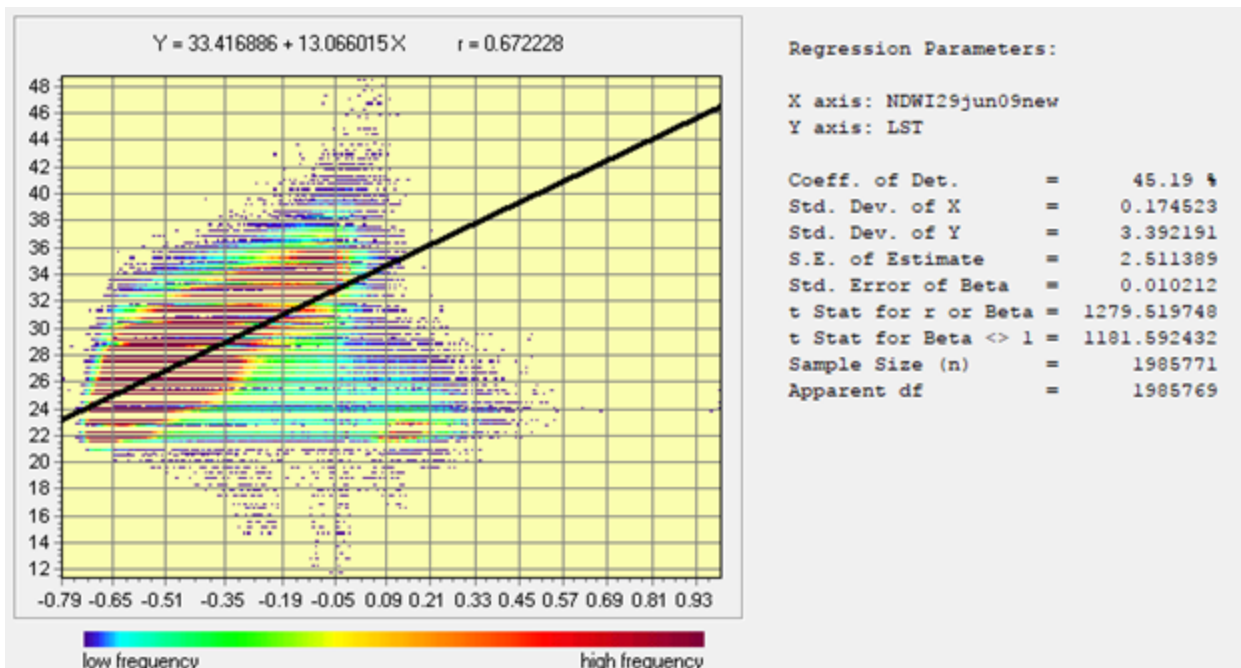
A6. 17 Aug 2015 - LST regressed on NDWI. Landsat 8 image.



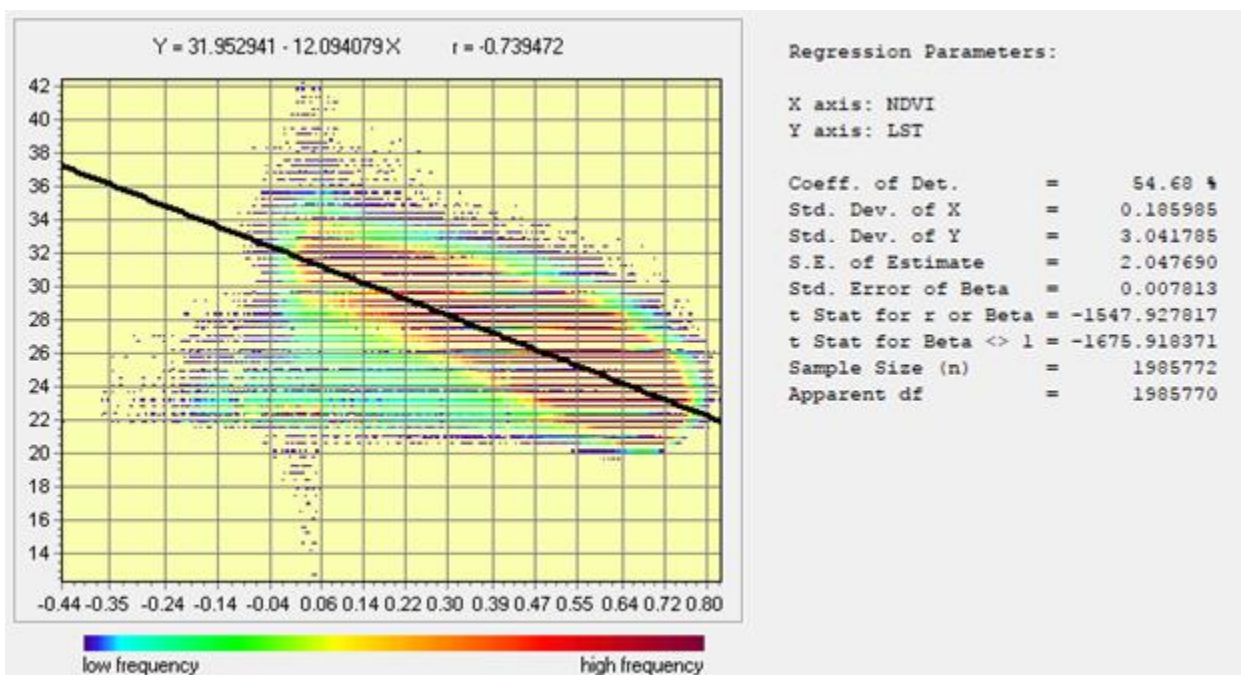
A7. 29 June 2009 - LST regressed on NDVI. Landsat 5 image.



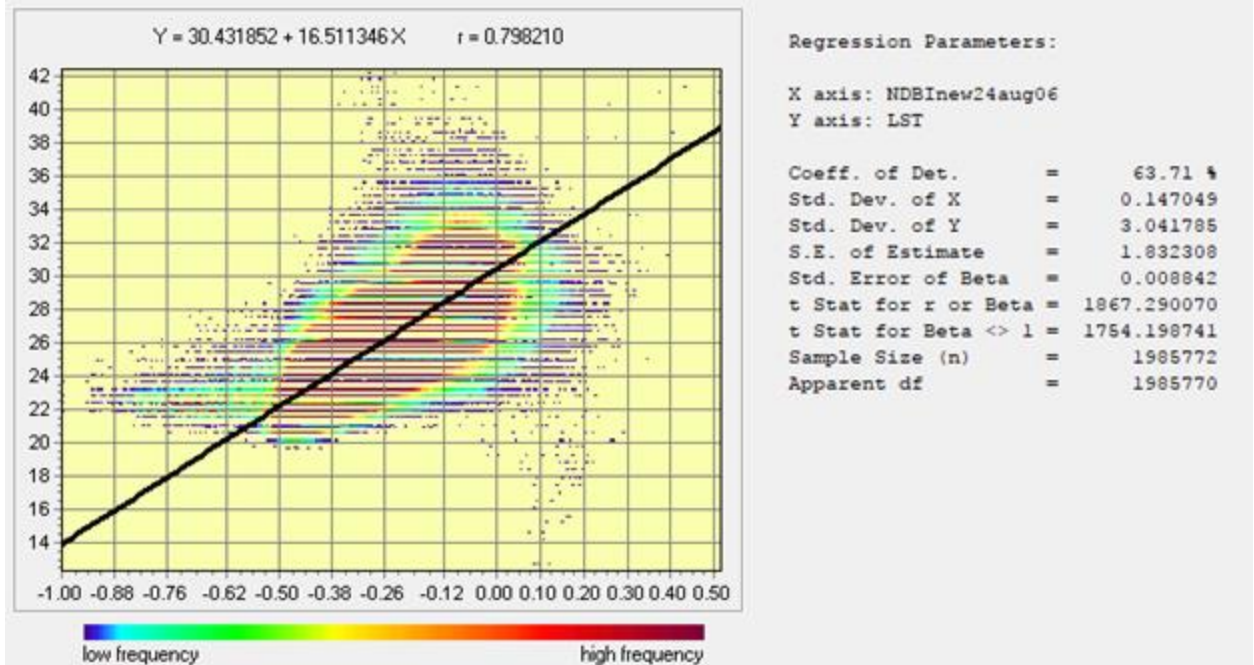
A7. 29 June 2009 - LST regressed on NDBI. Landsat 5 image.



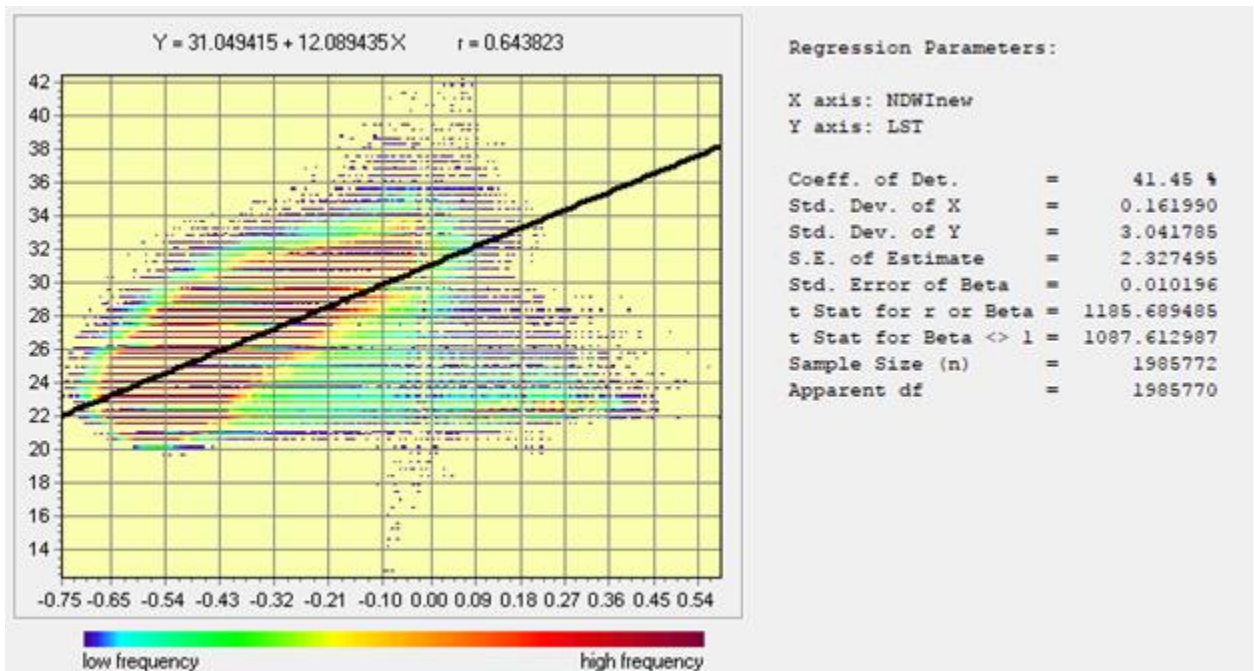
A7. 29 June 2009 - LST regressed on NDWI. Landsat 5 image.



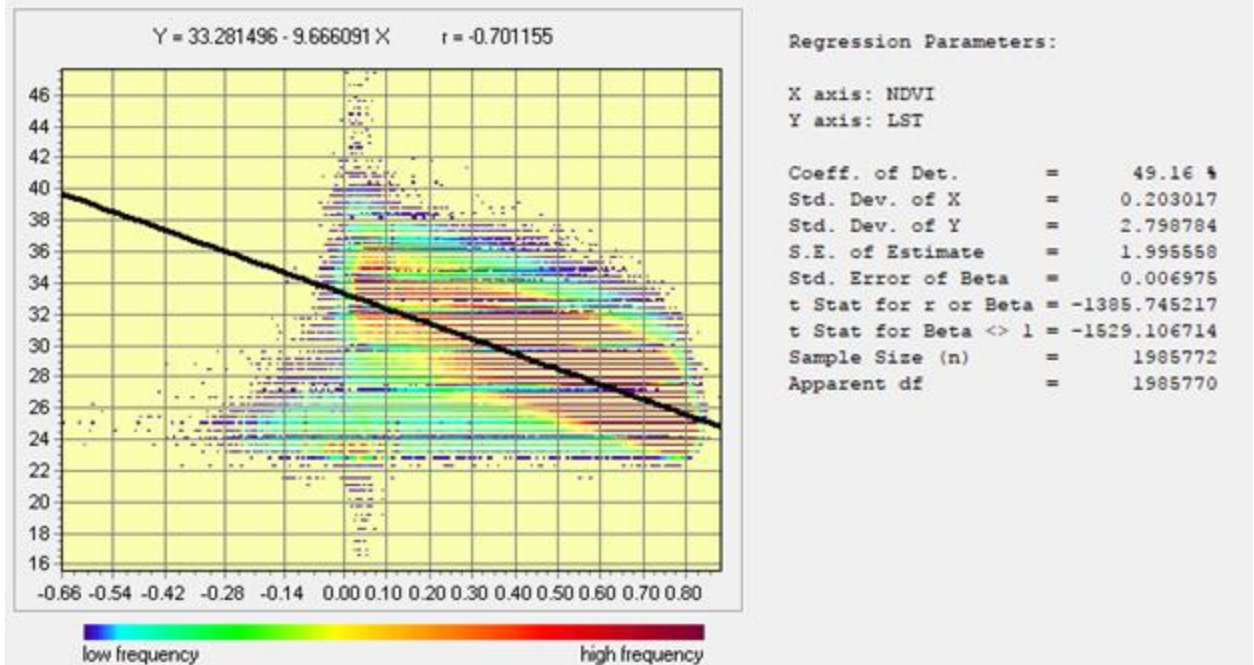
A8. 24 August 2006 - LST regressed on NDVI. Landsat 5 image.



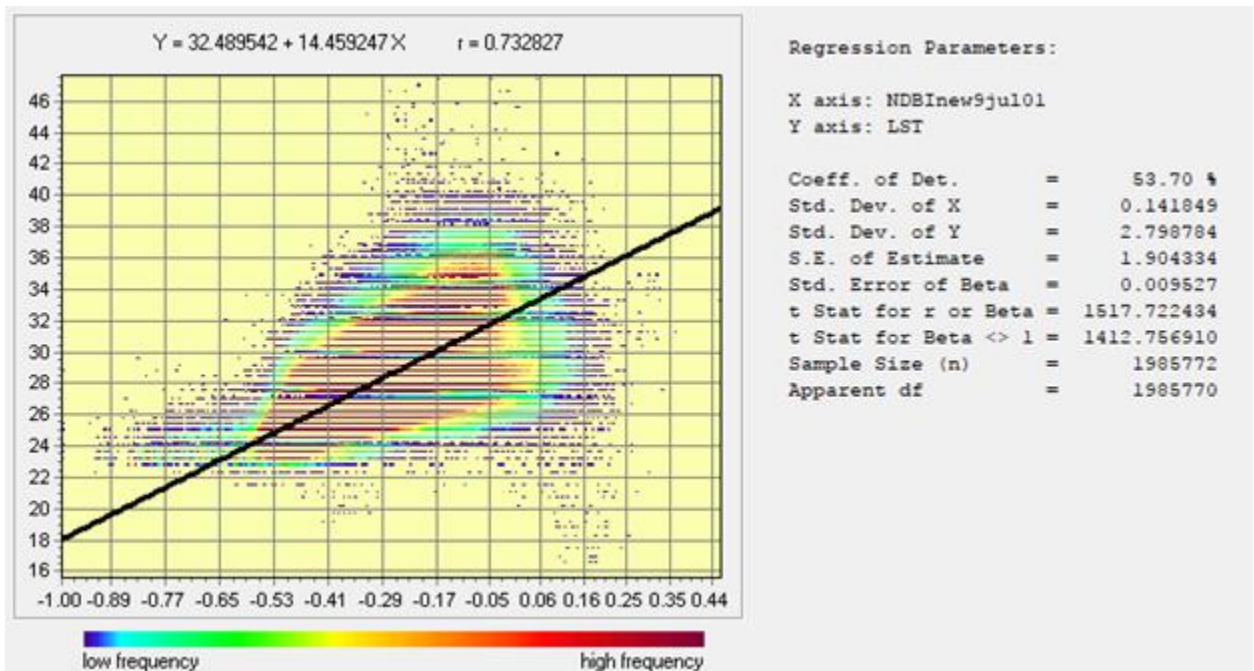
A9. 24 August 2006 - LST regressed on NDBI. Landsat 5 image.



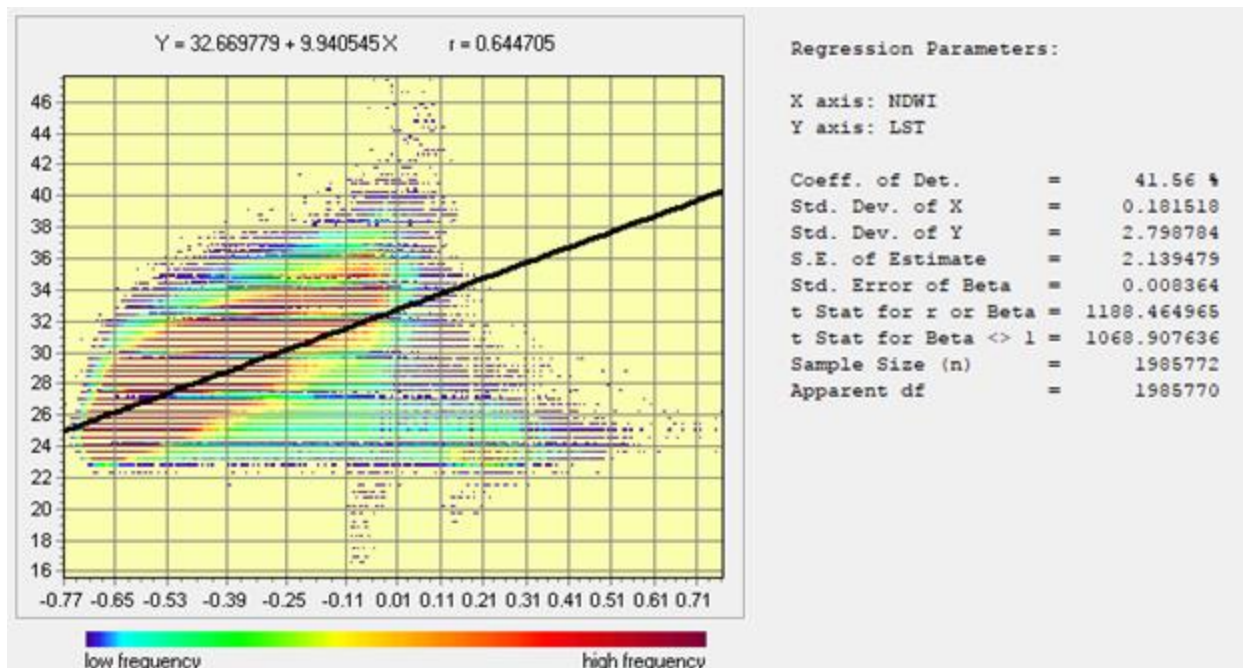
A10. 24 August 2006 - LST regressed on NDWI. Landsat 5 image.



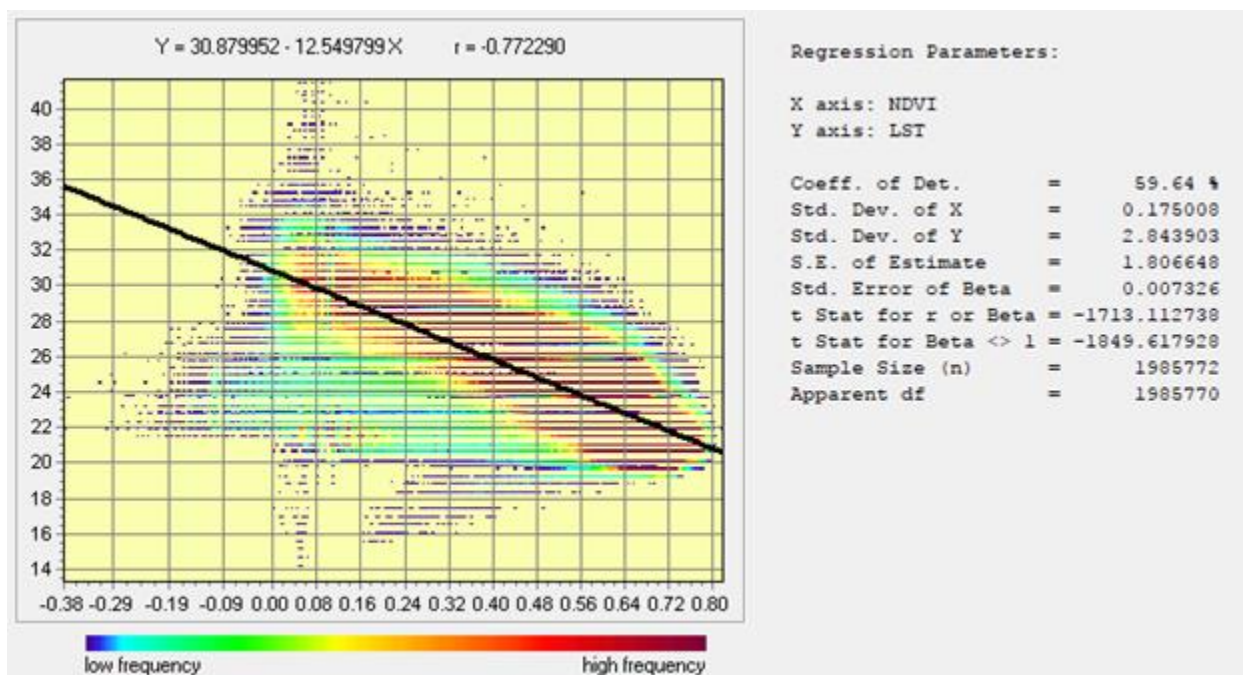
A11. 09 July 2001 - LST regressed on NDVI. Landsat 5 image.



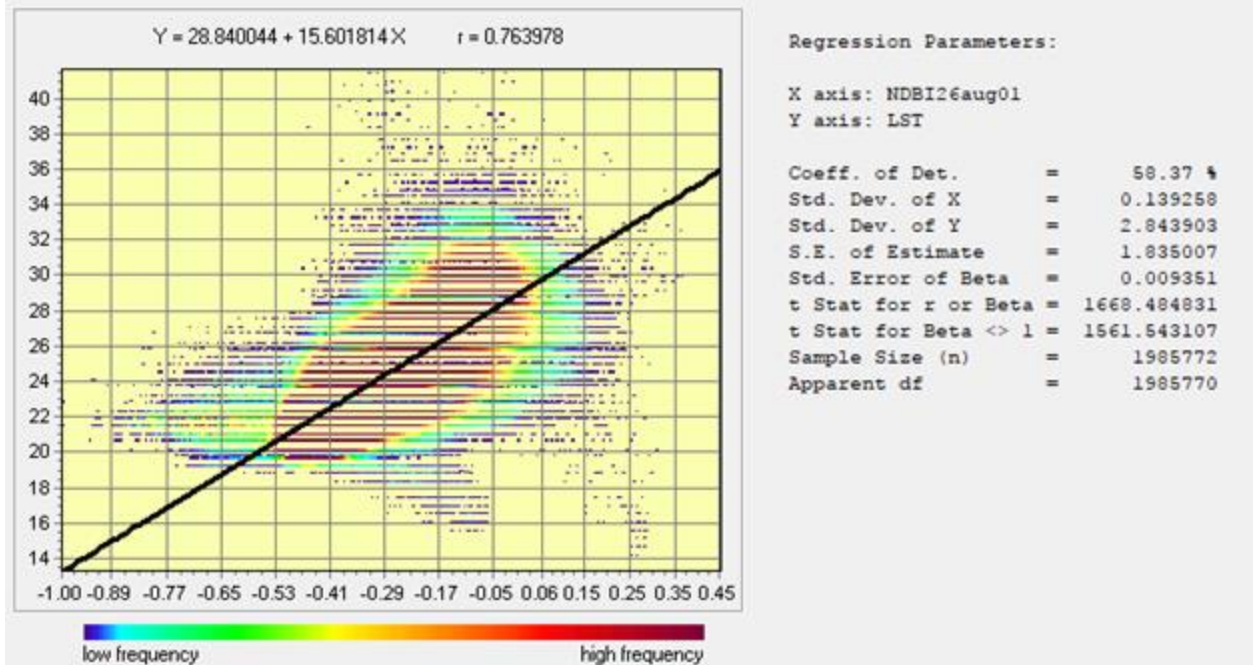
A12. 09 July 2001 - LST regressed on NDBI. Landsat 5 image.



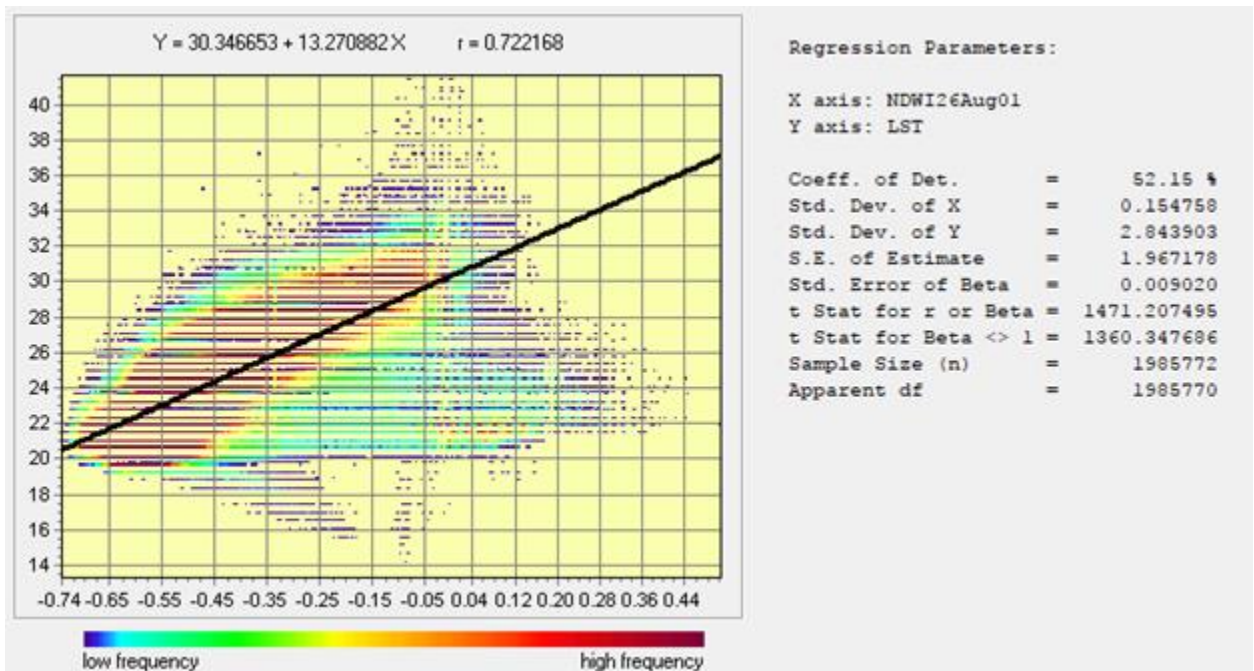
A13. 09 July 2001 - LST regressed on NDWI. Landsat 5 image.



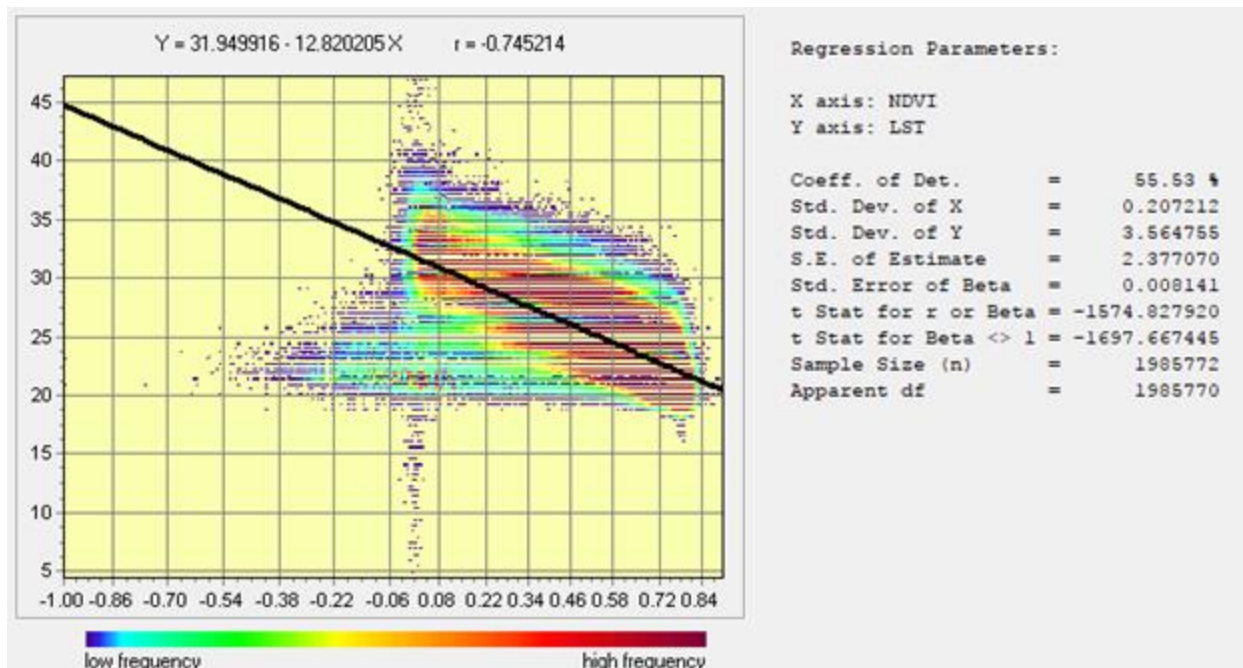
A14. 26 August 2001 - LST regressed on NDVI. Landsat 5 image.



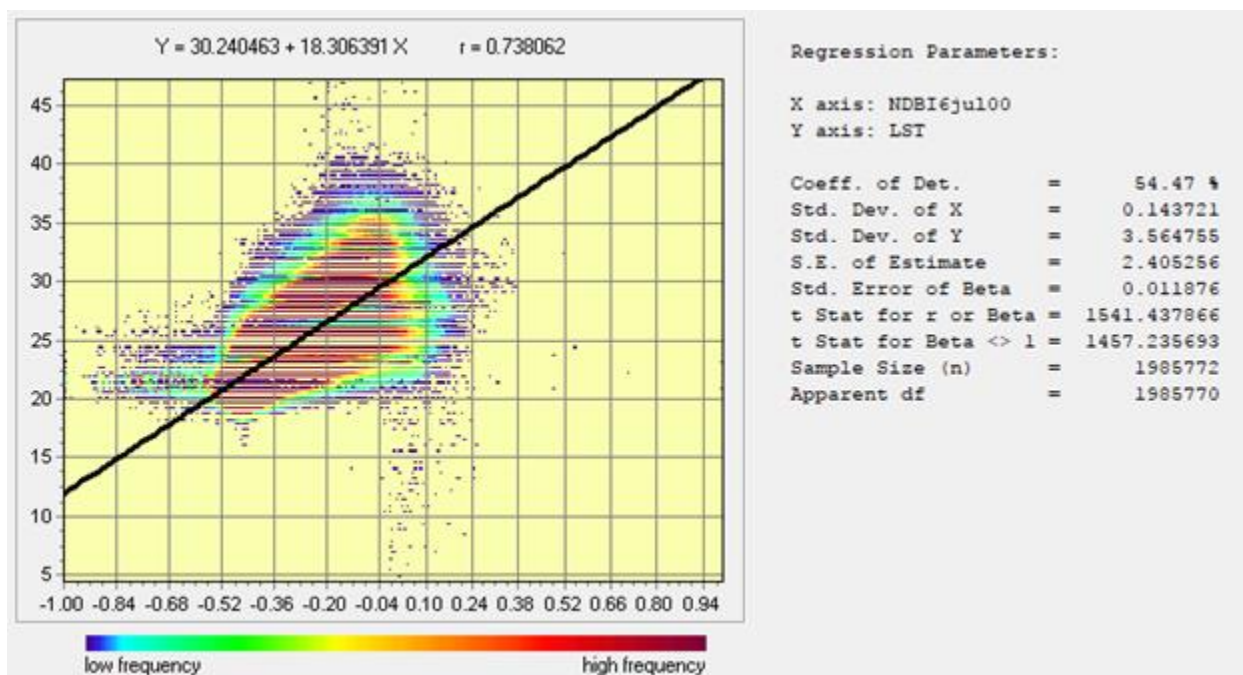
A15. 26 August 2001 - LST regressed on NDBI. Landsat 5 image.



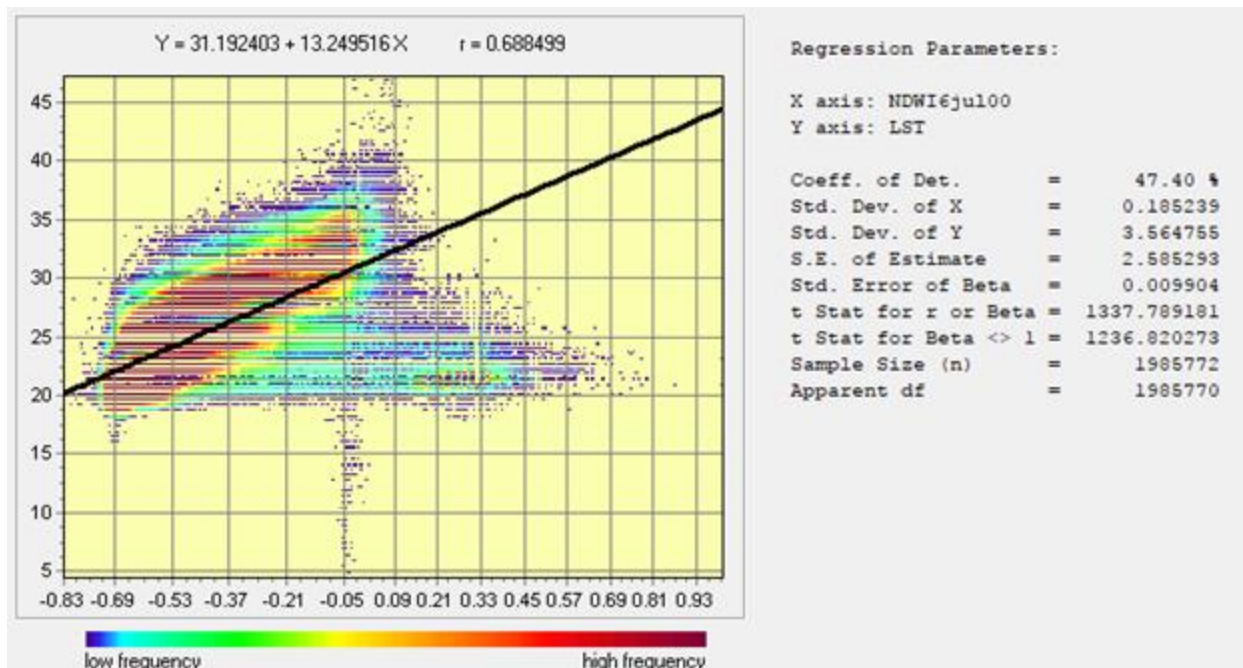
A16. 26 August 2001 - LST regressed on NDWI. Landsat 5 image.



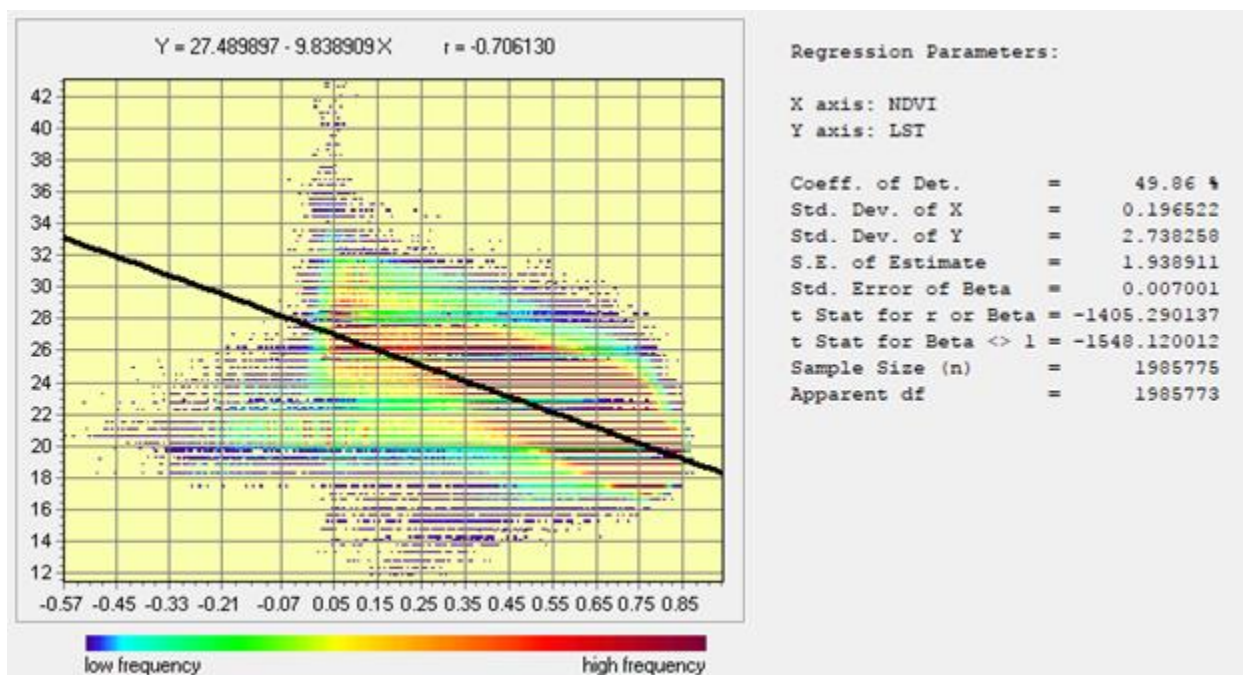
A17. 6 July 2000 - LST regressed on NDVI. Landsat 5 image.



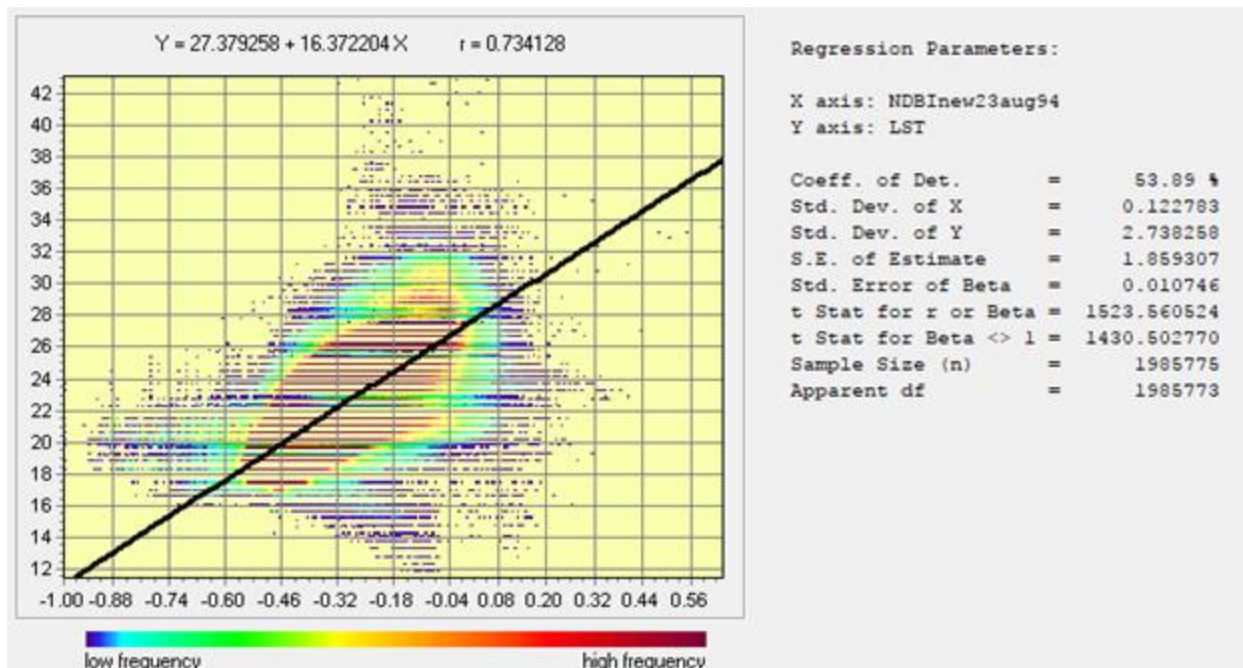
A18. 6 July 2000 - LST regressed on NDBI. Landsat 5 image.



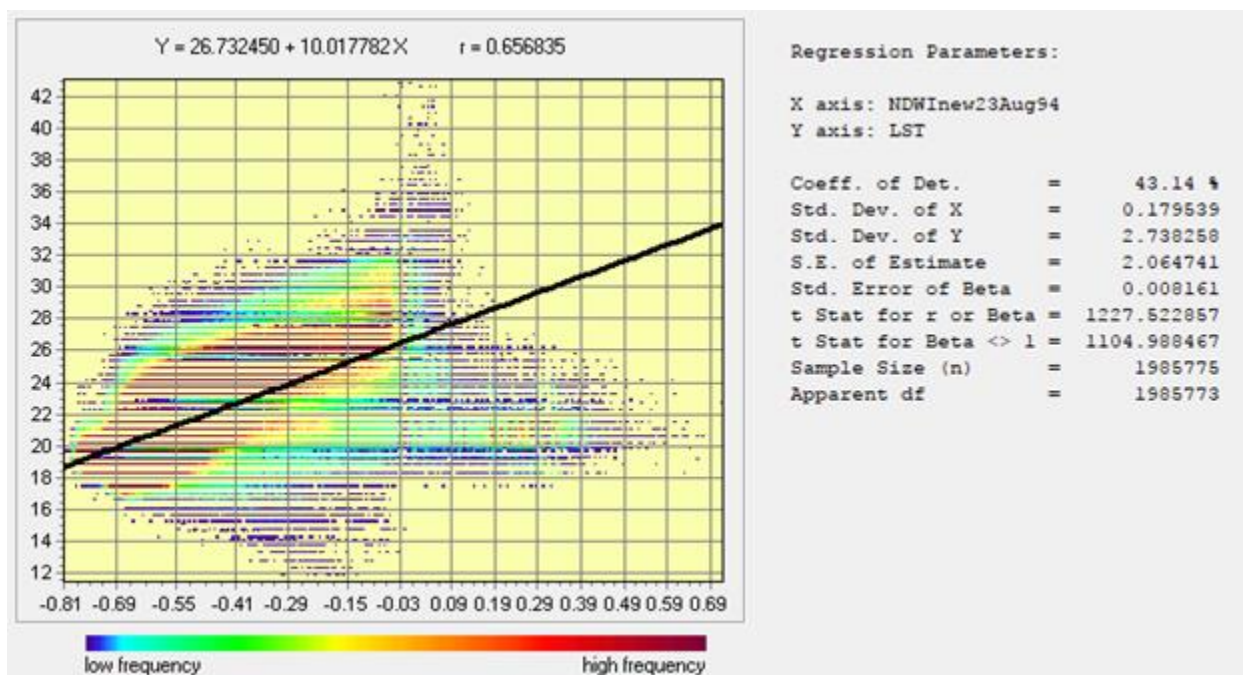
A19. 6 July 2000 - LST regressed on NDWI. Landsat 5 image.



A20. 6 July 2000 - LST regressed on NDVI. Landsat 5 image.



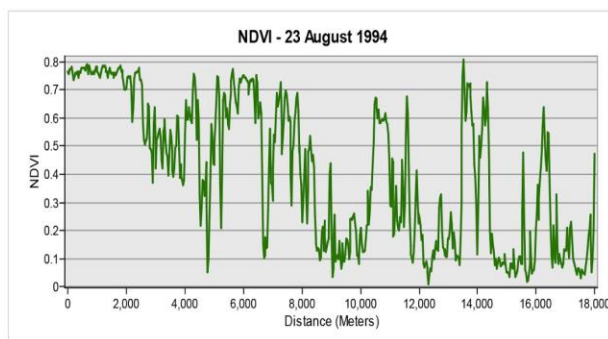
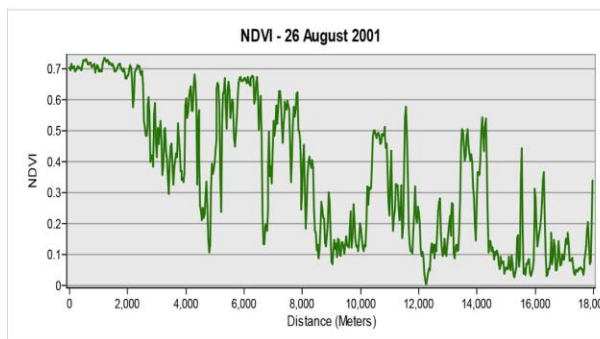
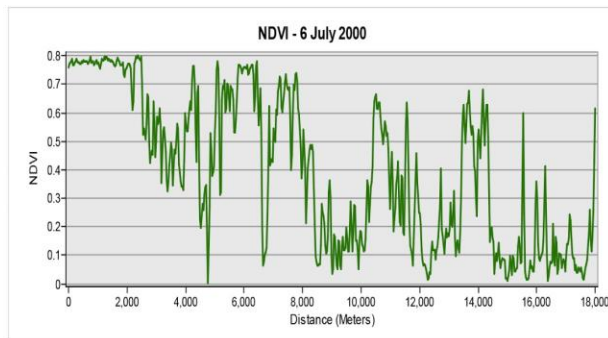
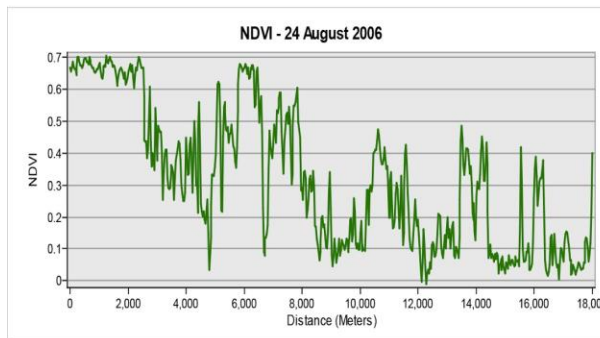
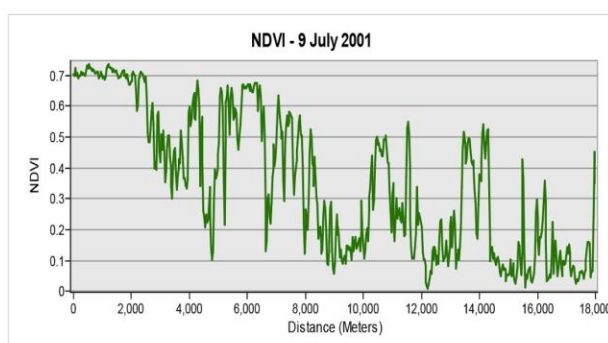
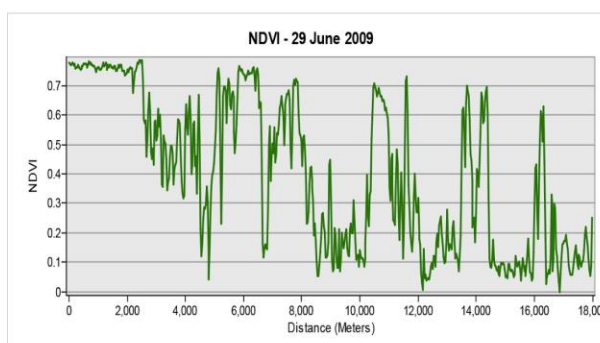
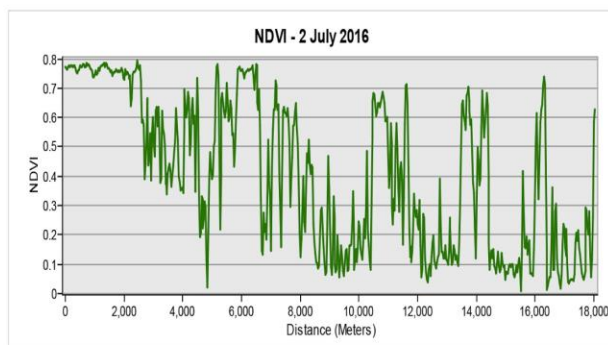
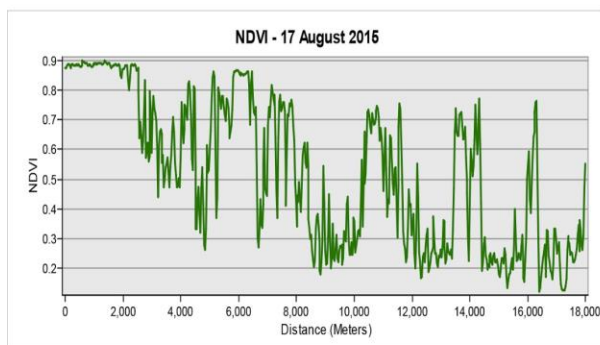
A21. 6 July 2000 - LST regressed on NDBI. Landsat 5 image.



A22. 6 July 2000 - LST regressed on NDWI. Landsat 5 image.

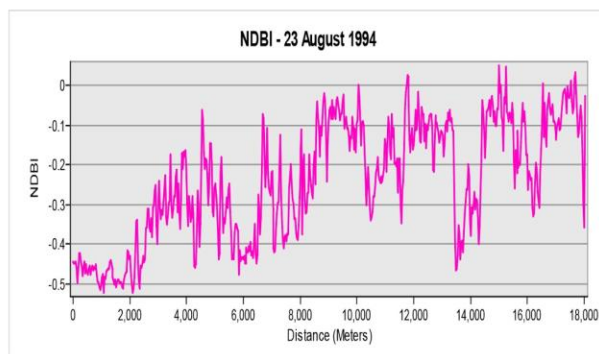
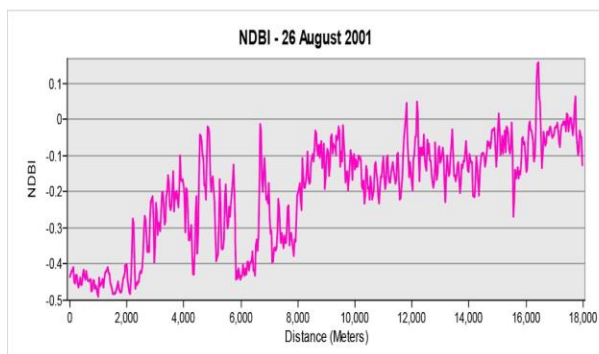
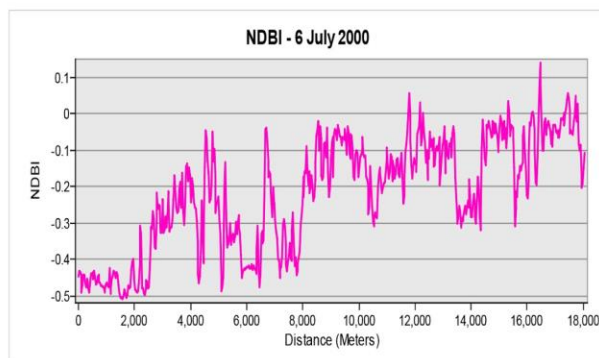
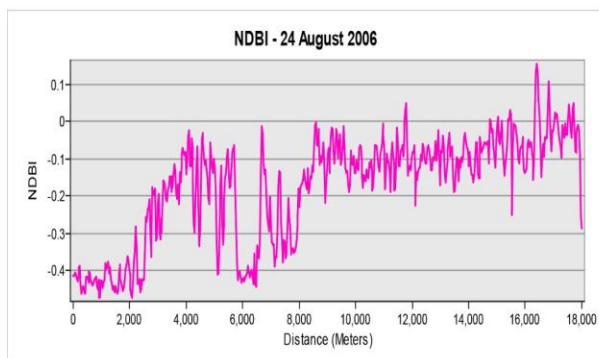
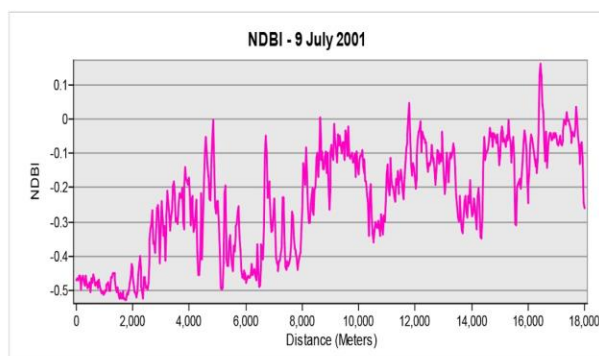
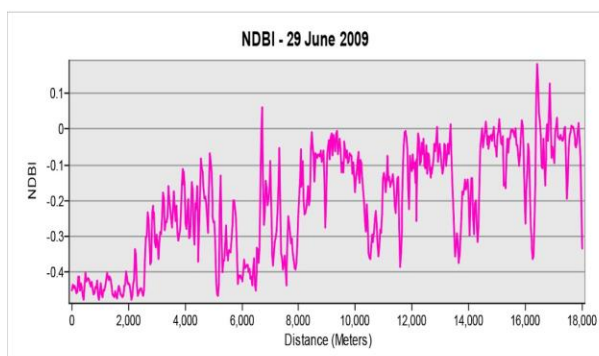
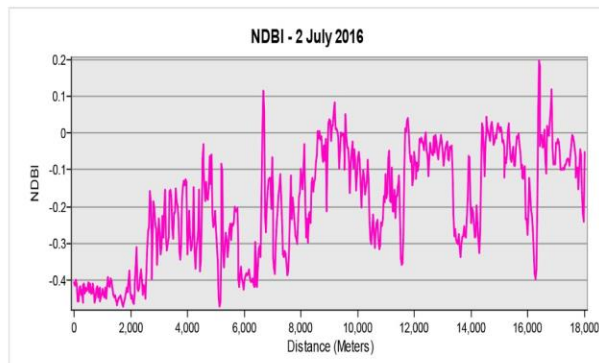
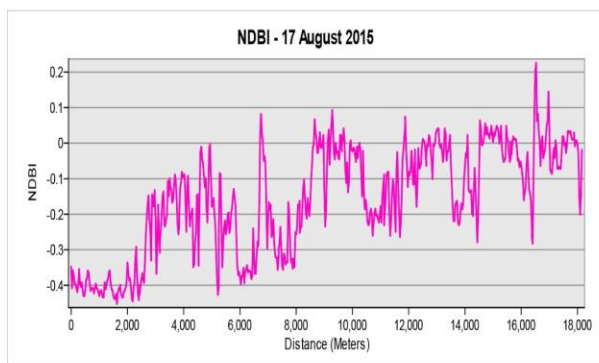
Appendix B

NDVI Transects



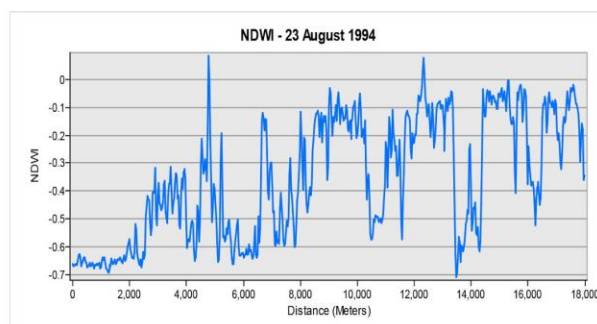
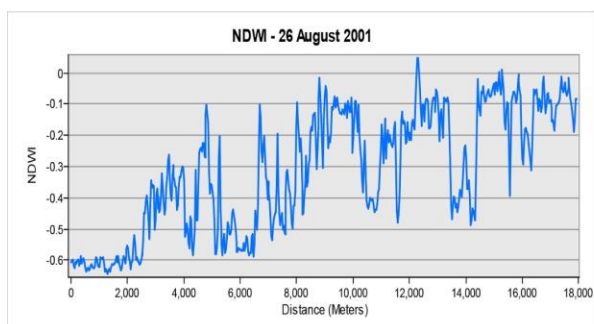
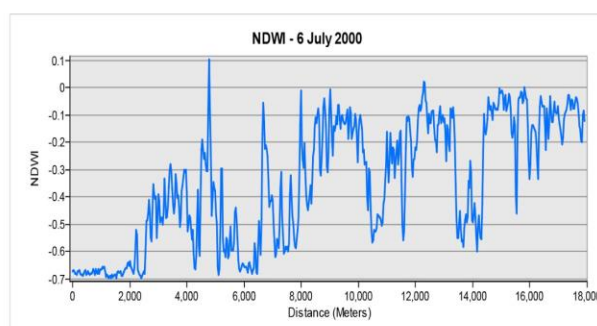
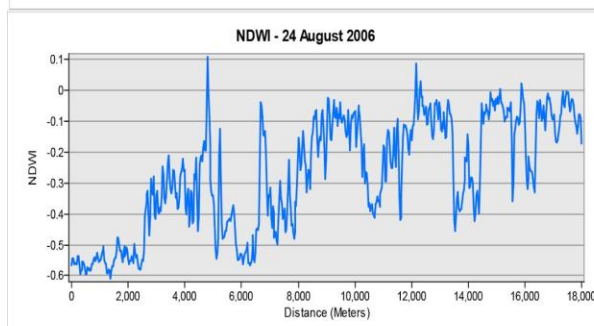
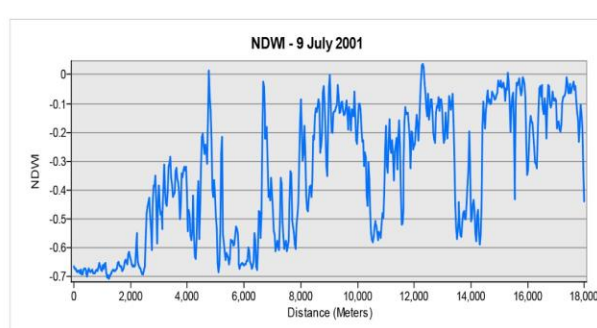
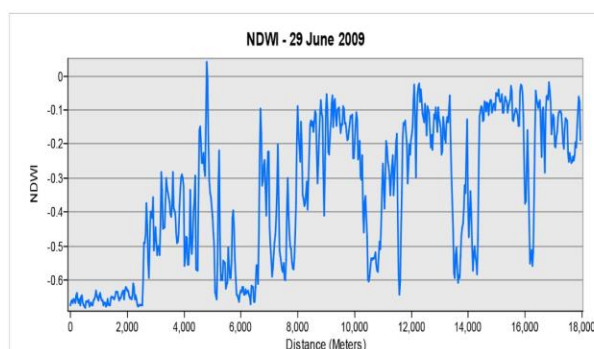
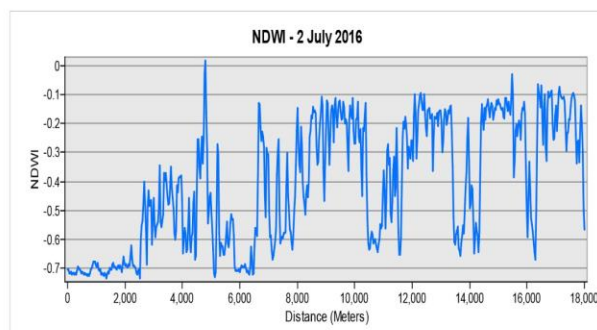
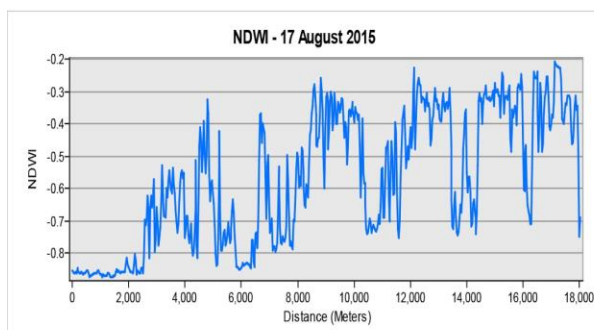
B1. NDVI transects for all selected scenes.

NDBI Transects



B2. NDBI transects for all selected scenes.

NDWI Transects



B3. NDWI transects for all selected scenes.

Literature Cited

- Alghamdi, A. S., & Moore, T. W. (2015). Detecting Temporal Changes in Riyadh's Urban Heat Island. *Papers in Applied Geography*, 1(4), 312-325.
- Ali, J. M., Marsh, S. H., & Smith, M. J. (2017). A comparison between London and Baghdad surface urban heat islands and possible engineering mitigation solutions. *Sustainable Cities and Society*, 29, 159-168.
- Amiri, R., Weng, Q., Alimohammadi, A., & Alavipanah, S. K. (2009). Spatial-temporal dynamics of land surface temperature in relation to fractional vegetation cover and land use/cover in the Tabriz urban area, Iran. *Remote sensing of environment*, 113(12), 2606-2617.
- Anderson, G. B., & Bell, M. L. (2011). Heat waves in the United States: mortality risk during heat waves and effect modification by heat wave characteristics in 43 US communities. *Environmental health perspectives*, 119(2), 210.
- Arnfield, A. J. (2003). Two decades of urban climate research: a review of turbulence, exchanges of energy and water, and the urban heat island. *International journal of climatology*, 23(1), 1-26.
- Bahi, H., Rhinane, H., Bensalmia, A., Fehrenbach, U., & Scherer, D. (2016). Effects of urbanization and seasonal cycle on the surface urban heat island patterns in the coastal growing cities: A case study of Casablanca, Morocco. *Remote Sensing*, 8(10), 829.
- Balling Jr, R. C., & Brazel, S. W. (1987). Time and space characteristics of the Phoenix urban heat island. *Journal of the Arizona-Nevada Academy of Science*, 75-81.
- Battaglia, M., Buckley, G., Galvin, M., & Grove, M. (2014). It's not easy going green: obstacles to tree-planting programs in East Baltimore.
- Becker, F., & Li, Z. L. (1990). Towards a local split window method over land surfaces. *Remote Sensing*, 11(3), 369-393.
- Becker, F., & Li, Z. L. (1995). Surface temperature and emissivity at various scales: Definition, measurement and related problems. *Remote Sensing Reviews*, 12(3-4), 225-253.
- Bornstein, R. D. (1968). Observations of the urban heat island effect in New York City. *Journal of Applied Meteorology*, 7(4), 575-582.
- Bounoua, L., Safia, A., Masek, J., Peters-Lidard, C., & Imhoff, M. L. (2009). Impact of urban growth on surface climate: A case study in Oran, Algeria. *Journal of applied meteorology and climatology*, 48(2), 217-231.

- Bounoua, L., Zhang, P., Nigro, J., Lachir, A., & Thome, K. (2017). Regional Impacts of Urbanization in the United States. *Canadian Journal of Remote Sensing*, (just-accepted), 00-00.
- Buechley, R. W., Van Bruggen, J., & Truppi, L. E. (1972). Heat island= death island?. *Environmental Research*, 5(1), 85-92.2(1), 54-63.
- Busato, F., Lazzarin, R. M., & Noro, M. (2014). Three years of study of the Urban Heat Island in Padua: Experimental results. *Sustainable Cities and Society*, 10, 251-258.
- Carlson, T. N., & Arthur, S. T. (2000). The impact of land use—land cover changes due to urbanization on surface microclimate and hydrology: a satellite perspective. *Global and Planetary Change*, 25(1), 49-65.
- CDC (Centers for Disease Control) (2006) Heat-related Deaths---United States, 1999–2003, Mortality and Morbidity Weekly Report published by the Centers for Disease Control, July 28, 2006/55(29):796–798
- Chen, X. L., Zhao, H. M., Li, P. X., & Yin, Z. Y. (2006). Remote sensing image-based analysis of the relationship between urban heat island and land use/cover changes. *Remote sensing of environment*, 104(2), 133-146.
- Cui, Y. Y., & De Foy, B. (2012). Seasonal variations of the urban heat island at the surface and the near-surface and reductions due to urban vegetation in Mexico City. *Journal of Applied Meteorology and Climatology*, 51(5), 855-868.
- Deng, C., & Wu, C. (2013). Examining the impacts of urban biophysical compositions on surface urban heat island: A spectral unmixing and thermal mixing approach. *Remote Sensing of Environment*, 131, 262-274.
- Eastman, J.R. (2016). TerrSet [Computer Software]. Worcester, MA: Clark University
- Effat, H. A., & Hassan, O. A. K. (2014). Change detection of urban heat islands and some related parameters using multi-temporal Landsat images; a case study for Cairo city, Egypt. *Urban Climate*, 10, 171-188.
- Fischer, E. M., Oleson, K. W., & Lawrence, D. M. (2012). Contrasting urban and rural heat stress responses to climate change. *Geophysical research letters*, 39(3).
- Gaffin, S. R., Rosenzweig, C., Khanbilvardi, R., Parshall, L., Mahani, S., Glickman, H., ... & Hillel, D. (2008). Variations in New York city's urban heat island strength over time and space. *Theoretical and applied climatology*, 94(1), 1-11.

- Grimmond, S. (2007). Urbanization and global environmental change: local effects of urban warming. *The Geographical Journal*, 173(1), 83-88.
- Grundstein, A., & Dowd, J. (2011). Trends in extreme apparent temperatures over the United States, 1949–2010. *Journal of Applied Meteorology and Climatology*, 50(8), 1650-1653.
- H. Yamagata, M. Nasu, M. Yoshizawa, A. Miyamoto, and M. Minamiyama, “Heat island mitigation using water retentive pavement sprinkled with reclaimed wastewater,” *Water Sci. Technol. a J. Int. Assoc. Water Pollut. Res.*, vol. 57, no. 5, pp. 763–771, Jan. 2008.
- Hafner, J., & Kidder, S. Q. (1999). Urban heat island modeling in conjunction with satellite-derived surface/soil parameters. *Journal of applied meteorology*, 38(4), 448-465.
- Han-qiu, X., & Ben-qing, C. (2004). Remote sensing of the urban heat island and its changes in Xiamen City of SE China. *Journal of Environmental Sciences*, 16(2), 276-281.
- Hardin, A. W., Liu, Y., Cao, G., & Vanos, J. K. (2017). Urban heat island intensity and spatial variability by synoptic weather type in the northeast US. *Urban Climate*.
- Harlan, S. L., Brazel, A. J., Darrel Jenerette, G., Jones, N. S., Larsen, L., Prashad, L., & Stefanov, W. L. (2007). In the shade of affluence: the inequitable distribution of the urban heat island. In *Equity and the Environment* (pp. 173-202). Emerald Group Publishing Limited.
- Hart, M. A., & Sailor, D. J. (2009). Quantifying the influence of land-use and surface characteristics on spatial variability in the urban heat island. *Theoretical and applied climatology*, 95(3-4), 397-406.
- Hendel, M., Colombert, M., Diab, Y., & Royon, L. (2014). Improving a pavement-watering method on the basis of pavement surface temperature measurements. *Urban Climate*, 10, 189-200.
- Howard, L. (1818). *The climate of London* (Vol. 1). W. Phillips, sold also by J. and A. Arch.
- Hu, L., & Brunsell, N. A. (2013). The impact of temporal aggregation of land surface temperature data for surface urban heat island (SUHI) monitoring. *Remote Sensing of Environment*, 134, 162-174.

- Huang, G., Zhou, W., & Cadenasso, M. L. (2011). Is everyone hot in the city? Spatial pattern of land surface temperatures, land cover and neighborhood socioeconomic characteristics in Baltimore, MD. *Journal of environmental management*, 92(7), 1753-1759.
- Heusinkveld, B. G., Steeneveld, G. J., Hove, L. V., Jacobs, C. M. J., & Holtslag, A. A. M. (2014). Spatial variability of the Rotterdam urban heat island as influenced by urban land use. *Journal of Geophysical Research: Atmospheres*, 119(2), 677-692.
- Imhoff, M. L., Zhang, P., Wolfe, R. E., & Bounoua, L. (2010). Remote sensing of the urban heat island effect across biomes in the continental USA. *Remote Sensing of Environment*, 114(3), 504-513.
- Lazzarini, M., Marpu, P. R., & Ghedira, H. (2013). Temperature-land cover interactions: The inversion of urban heat island phenomenon in desert city areas. *Remote Sensing of Environment*, 130, 136-152.
- Luber, G., & McGeehin, M. (2008). Climate change and extreme heat events. *American journal of preventive medicine*, 35(5), 429-435.
- Li, D., & Bou-Zeid, E. (2013). Synergistic interactions between urban heat islands and heat waves: the impact in cities is larger than the sum of its parts. *Journal of Applied Meteorology and Climatology*, 52(9), 2051-2064.
- Li, Y. Y., Zhang, H., & Kainz, W. (2012). Monitoring patterns of urban heat islands of the fast-growing Shanghai metropolis, China: Using time-series of Landsat TM/ETM+ data. *International Journal of Applied Earth Observation and Geoinformation*, 19, 127-138.
- Liu, L., & Zhang, Y. (2011). Urban heat island analysis using the Landsat TM data and ASTER data: A case study in Hong Kong. *Remote Sensing*, 3(7), 1535-1552.
- Lu, D., & Weng, Q. (2006). Use of impervious surface in urban land-use classification. *Remote Sensing of Environment*, 102(1), 146-160.
- Mahmood, R., Pielke, R. A., Hubbard, K. G., Niyogi, D., Dirmeyer, P. A., McAlpine, C., ... & Baker, B. (2014). Land cover changes and their biogeophysical effects on climate. *International Journal of Climatology*, 34(4), 929-953.
- Mathew, A., Khandelwal, S., & Kaul, N. (2017). Investigating spatial and seasonal variations of urban heat island effect over Jaipur city and its relationship with vegetation, urbanization and elevation parameters. *Sustainable Cities and Society*, 35, 157-177.
- Matson, M., McClain, E. P., McGinnis Jr, D. F., & Pritchard, J. A. (1978). Satellite detection of urban heat islands. *Monthly Weather Review*, 106(12), 1725-1734.

- McFeeters, S. K. (1996). The use of the Normalized Difference Water Index (NDWI) in the \delineation of open water features. *International journal of remote sensing*, 17(7), 1425-1432.
- Miao, S., Chen, F., LeMone, M. A., Tewari, M., Li, Q., & Wang, Y. (2009). An observational and modeling study of characteristics of urban heat island and boundary layer structures in Beijing. *Journal of Applied Meteorology and Climatology*, 48(3), 484-501.
- Mills, G. (2014). Urban climatology: History, status and prospects. *Urban Climate*, 10, 479-489.
- Mirzaei, P. A., & Haghighat, F. (2010). Approaches to study urban heat island–abilities and limitations. *Building and Environment*, 45(10), 2192-2201.
- Mitraka, Z., Chrysoulakis, N., Doxani, G., Del Frate, F., & Berger, M. (2015). Urban surface temperature time series estimation at the local scale by spatial-spectral unmixing of satellite observations. *Remote Sensing*, 7(4), 4139-4156.
- Myrup, L. O. (1969). A numerical model of the urban heat island. *Journal of Applied Meteorology*, 8(6), 908-918.
- Nakayama, T., & Fujita, T. (2010). Cooling effect of water-holding pavements made of new materials on water and heat budgets in urban areas. *Landscape and urban planning*, 96(2), 57-67.
- Nassar, A. K., Blackburn, G. A., & Whyatt, J. D. (2016). Dynamics and controls of urban heat sink and island phenomena in a desert city: Development of a local climate zone scheme using remotely-sensed inputs. *International journal of applied earth observation and geoinformation*, 51, 76-90.
- Ngie, A., Abutaleb, K., Ahmed, F., Darwish, A., & Ahmed, M. (2014). Assessment of urban heat island using satellite remotely sensed imagery: a review. *South African Geographical Journal*, 96(2), 198-214.
- Noro, M., Busato, F., & Lazzarin, R. M. (2015). Urban heat island in Padua, Italy: Experimental and theoretical analysis. *Indoor and Built Environment*, 24(4), 514-533.
- Oke, T. R. (1973). City size and the urban heat island. *Atmospheric Environment (1967)*, 7(8), 769-779.
- Oke, T. R. (1988). The urban energy balance. *Progress in Physical geography*, 12(4), 471-508.

- Pearsall, H. (2017). Staying cool in the compact city: Vacant land and urban heating in Philadelphia, Pennsylvania. *Applied Geography*, 79, 84-92.
- Peng, S., Piao, S., Ciais, P., Friedlingstein, P., Ottle, C., Bréon, F. M., ... & Myneni, R. B. (2011). Surface urban heat island across 419 global big cities. *Environmental science & technology*, 46(2), 696-703.
- Picón, A. J., Vásquez, R., González, J., Luvall, J., & Rickman, D. (2017). Use of remote sensing observations to study the urban climate on tropical coastal cities. *Revista Umbral (Etapa IV-Colección completa)*, (1), 218-232.
- Rajasekar, U., & Weng, Q. (2009). Urban heat island monitoring and analysis using a non-parametric model: A case study of Indianapolis. *ISPRS Journal of Photogrammetry and Remote Sensing*, 64(1), 86-96.
- Rao, P. K. (1972). Remote sensing of urban heat islands from an environmental satellite. *Bulletin of the American Meteorological Society*, 53(7), 647.
- Rey, G., Jougl, E., Fouillet, A., Pavillon, G., Bessemoulin, P., Frayssinet, P., ... & Hémon, D. (2007). The impact of major heat waves on all-cause and cause-specific mortality in France from 1971 to 2003. *International archives of occupational and environmental health*, 80(7), 615-626.
- Rinner, C., & Hussain, M. (2011). Toronto's urban heat island—Exploring the relationship between land use and surface temperature. *Remote Sensing*, 3(6), 1251-1265.
- Rivera, E., Antonio-Némiga, X., Origel-Gutiérrez, G., Sarricolea, P., & Adame-Martínez, S. (2017). Spatiotemporal analysis of the atmospheric and surface urban heat islands of the Metropolitan Area of Toluca, Mexico. *Environmental Earth Sciences*, 76(5), 225.
- Rizwan, A. M., Dennis, L. Y., & Chunho, L. I. U. (2008). A review on the generation, determination and mitigation of Urban Heat Island. *Journal of Environmental Sciences*, 20(1), 120-128.
- Robine, J. M., Cheung, S. L. K., Le Roy, S., Van Oyen, H., Griffiths, C., Michel, J. P., & Herrmann, F. R. (2008). Death toll exceeded 70,000 in Europe during the summer of 2003. *Comptes rendus biologies*, 331(2), 171-178.
- Romero-Lankao, P., Qin, H., & Dickinson, K. (2012). Urban vulnerability to temperature-related hazards: A meta-analysis and meta-knowledge approach. *Global Environmental Change*, 22(3), 670-683.
- Roy, D. P., Wulder, M. A., Loveland, T. R., Woodcock, C. E., Allen, R. G., Anderson, M. C., ... & Scambos, T. A. (2014). Landsat-8: Science and product vision for terrestrial global change research. *Remote Sensing of Environment*, 145, 154-172.

- Scott, A. A., Zaitchik, B., Waugh, D. W., & O'Meara, K. (2017). Intraurban temperature variability in Baltimore. *Journal of Applied Meteorology and Climatology*, 56(1), 159-171.
- Sheridan, S. C., & Dixon, P. G. (2016). Spatiotemporal trends in human vulnerability and adaptation to heat across the United States. *Anthropocene*.
- Sobrino, J. A., Oltra-Carrió, R., Sòria, G., Jiménez-Muñoz, J. C., Franch, B., Hidalgo, V., & Gómez, J. A. (2013). Evaluation of the surface urban heat island effect in the city of Madrid by thermal remote sensing. *International journal of remote sensing*, 34(9-10), 3177-3192.
- Souch, C., & Grimmond, S. (2006). Applied climatology: urban climate. *Progress in physical geography*, 30(2), 270-279.
- Steenekveld, G. J., Koopmans, S., Heusinkveld, B. G., Van Hove, L. W. A., & Holtslag, A. A. M. (2011). Quantifying urban heat island effects and human comfort for cities of variable size and urban morphology in the Netherlands. *Journal of Geophysical Research: Atmospheres*, 116(D20).
- Stewart, I. D., & Oke, T. R. (2012). Local climate zones for urban temperature studies. *Bulletin of the American Meteorological Society*, 93(12), 1879-1900.
- Stocker, T. (Ed.). (IPCC). (2014). *Climate change 2013: the physical science basis: Working Group I contribution to the Fifth assessment report of the Intergovernmental Panel on Climate Change*. Cambridge University Press.
- Stone, B. (2007). Urban and rural temperature trends in proximity to large US cities: 1951–2000. *International Journal of Climatology*, 27(13), 1801-1807.
- Stone, B., Hess, J. J., & Frumkin, H. (2010). Urban form and extreme heat events: are sprawling cities more vulnerable to climate change than compact cities. *Environmental health perspectives*, 118(10), 1425-1428.
- Streutker, D. R. (2003). Satellite-measured growth of the urban heat island of Houston, Texas. *Remote Sensing of Environment*, 85(3), 282-289.
- Schwarz, N., Schlink, U., Franck, U., & Großmann, K. (2012). Relationship of land surface and air temperatures and its implications for quantifying urban heat island indicators—An application for the city of Leipzig (Germany). *Ecological Indicators*, 18, 693-704.

- Sun, D., & Kafatos, M. (2007). Note on the NDVI-LST relationship and the use of temperature-related drought indices over North America. *Geophysical Research Letters*, 34(24).
- Sun, Q., Wu, Z., & Tan, J. (2012). The relationship between land surface temperature and land use/land cover in Guangzhou, China. *Environmental Earth Sciences*, 65(6), 1687-1694.
- Taha, H. (1997). Urban climates and heat islands: albedo, evapotranspiration, and anthropogenic heat. *Energy and buildings*, 25(2), 99-103.
- Tang, J., Di, L., Xiao, J., Lu, D., & Zhou, Y. (2017). Impacts of land use and socioeconomic patterns on urban heat Island. *International Journal of Remote Sensing*, 38(11), 3445-3465.
- Tomlinson, C. J., Chapman, L., Thornes, J. E., & Baker, C. (2011). Remote sensing land surface temperature for meteorology and climatology: A review. *Meteorological Applications*, 18(3), 296-306.
- Uejio, C. K., Wilhelmi, O. V., Golden, J. S., Mills, D. M., Gulino, S. P., & Samenow, J. P. (2011). Intra-urban societal vulnerability to extreme heat: the role of heat exposure and the built environment, socioeconomics, and neighborhood stability. *Health & Place*, 17(2), 498-507.
- United Nations. (2014). Department of Economic and Social Affairs, Population Division World Urbanization Prospects: The 2014 Revision, Highlights (ST/ESA/SER.A/352).
- USGS. (2016). *Landsat Collections*. Retrieved from <http://landsat.usgs.gov/landsat-collections>.
- Voiland, Adam. (2010). *Satellites Pinpoint Drivers of Urban Heat Islands in the Northeast*. Retrieved from <https://www.nasa.gov/topics/earth/features/heat-island-sprawl.html>
- Voogt, J. A., & Oke, T. R. (2003). Thermal remote sensing of urban climates. *Remote sensing of environment*, 86(3), 370-384.
- Wang, J., Huang, B., Fu, D., & Atkinson, P. M. (2015). Spatiotemporal variation in surface urban heat island intensity and associated determinants across major Chinese cities. *Remote Sensing*, 7(4), 3670-3689.
- Weng, Q., Lu, D., & Schubring, J. (2004). Estimation of land surface temperature-vegetation abundance relationship for urban heat island studies. *Remote sensing of Environment*, 89(4), 467-483.

- Wilby, R. L. (2003). Past and projected trends in London's urban heat island. *Weather*, 58(7), 251-260.
- Yuan, F., & Bauer, M. E. (2007). Comparison of impervious surface area and normalized difference vegetation index as indicators of surface urban heat island effects in Landsat imagery. *Remote sensing of Environment*, 106(3), 375-386.
- Zhang, et al., (2009). Bi-temporal characterization of land surface temperature in relation to impervious surface area, NDVI and NDBI, using a sub-pixel image analysis. *International Journal of Applied Earth Observation and Geoinformation*, 11(4), 256-264.
- Zhang, H., Qi, Z. F., Ye, X. Y., Cai, Y. B., Ma, W. C., & Chen, M. N. (2013). Analysis of land use/land cover change, population shift, and their effects on spatiotemporal patterns of urban heat islands in metropolitan Shanghai, China. *Applied Geography*, 44, 121-133.
- Zhou, W., Huang, G., & Cadenasso, M. L. (2011). Does spatial configuration matter? Understanding the effects of land cover pattern on land surface temperature in urban landscapes. *Landscape and Urban Planning*, 1
- Zhou, D., Zhao, S., Liu, S., Zhang, L., & Zhu, C. (2014). Surface urban heat island in China's 32 major cities: Spatial patterns and drivers. *Remote Sensing of Environment*, 152, 51-61.
- Zhou, W., Qian, Y., Li, X., Li, W., & Han, L. (2014). Relationships between land cover and the surface urban heat island: seasonal variability and effects of spatial and thematic resolution of land cover data on predicting land surface temperatures. *Landscape ecology*, 29(1), 153-167.
- Zinzi, M., & Carnielo, E. (2017). Impact of urban temperatures on energy performance and thermal comfort in residential buildings. The case of Rome, Italy. *Energy and Buildings*.

Curriculum Vitae

Education

Towson University, Towson, Maryland, 2016 – Present (Expected Conferral May 2018)
M.A. in Geography and Environmental Planning, thesis concentration: Urban
Climatology

California University of Pennsylvania, California, Pennsylvania, 2011-2016
B.S. in Earth Science, concentration in Geology
B.S. in Earth Science, concentration in Environmental Earth Science
Minor in Meteorology

Academic Employment

Teaching assistant: Department of Geography and Environmental Planning, Towson University (2016 – 2018)

- Grade labs, exams, and quizzes
- Assist students in Office hours
- In-class lectures when needed

Research assistant: Department of Geography and Environmental Planning, Towson University (Fall 2017)

- Produce land surface temperature (LST) and Normalized Difference Vegetation Index maps for Westminster, Maryland City Planner

Teaching assistant: Eberly Hall of Science and Technology, California University of Pennsylvania (2012 – 2016)

- Grade labs, exams, and quizzes
- Assist students when needed

Research Experience

Graduate Research

NASA DEVELOP National Program; NASA Goddard Space Flight Center
Greenbelt, MD, (Science Advisor Dr. John Bolton)

- Developed a global resiliency monitoring and measuring tool based on spatially continuous precipitation analysis
- Designed and coded a drought index based on the Sahel grasslands climate region
- Geospatial platforms used: Google Earth Engine, Google App Engine, ArcGIS

Long-term trend analysis and changes to the mean and variability of temperature in Pennsylvania from 1983 to 2014, 2016, Towson University (research adviser: Dr. Todd Moore)

- Examined trends and variability of precipitation in Pennsylvania using SPSS
- Baltimore City Urban Heat Island: A Problem Based Approach, 2016 (research adviser Dr. Todd W. Moore)
- Comprehensive examination of Baltimore City's urban heat island (UHI)
 - Examined differences between land cover indices, land surface temperatures, and several socioeconomic variables

Undergraduate Research

Department of Earth Science, California University of Pennsylvania, 2015; Carnegie Museum of Natural History (research adviser: Dr. Thomas Mueller).

- Investigating the Migration of Three Tree Species: Black Cherry, Red Maple, and Shagbark Hickory

National Oceanic and Atmospheric Administration; World Data Center for Paleoclimatology, 2014 (research adviser: Dr. David M. Anderson)

- Helped author and create a paleo resources catalog
- International project, talked with over 300 scientists from over 70 countries
- Gathered paleo resources, authored over 200 descriptions, and attended conferences

Department of Earth Science, California University of Pennsylvania, 2012 (research adviser: Dr. Thomas Mueller).

- Investigation of Southwest Pennsylvania using ArcGIS.
- Analysis of emergency operations buildings and their location with reference to stocked trout streams.
- Selected different locations with respect to their distance and driving times

NASA Space Grant Research Program, 2012 (research adviser: Dr. Thomas Mueller).

- In depth training on Unysis Integrated Data Viewer (IDV).
- Authoring of a step-by-step manual for the use of IDV by emergency managers.

Publications

Tomlin, J., El-Behaedi, R., Lingo, R., McCartney, S., Thieme, “Stress and Duress in the Sahel: Building Resiliency in Niger” Earthzine August (2017)

Anderson, David M., K. Horlick, and R. Lingo. “Share Your Geoscience Resources in the EarthCube Paleogeoscience Catalog.” Past Global Changes, PAGES June (2014): 1, Web.

Anderson, D., Horlick, K., Lingo, R., “NSF EarthCube Paleogeoscience RCN Catalog of Software Resources”, “NSF EarthCube Paleogeoscience RCN Catalog of Repository Resources”, and “NSF EarthCube Paleogeoscience RCN Catalog of Database Resources”, National Oceanic and Atmospheric Administration, 8/20/2014

